1 **SIZ1 is a nuclear host target of the nematode effector GpRbp1 from *Globodera pallida* that**

2 **acts as a negative regulator of basal plant defense to cyst nematodes**

3 **Authors**

4 Amalia Diaz-Granados[1]; Mark G. Sterken[1]; Jarno Persoon[1]; Hein Overmars[1]; Somnath S.

5 Pokhare[2]; Magdalena J Mazur[3]; Sergio Martin-Ramirez[1]; Martijn Holterman[1]; Eliza C. Martin[4];

6 Rikus Pomp[1]; Anna Finkers-Tomczak; Jan Roosien[1]; Abdenaser Elashry[2]; Florian Grundler[2];

7 Andrei J Petrescu[4]; Geert Smant[1]; Aska Goverse[1]

8

9 **Author's affiliations:**

10 1-Laboratory of Nematology, Wageningen University and Research, Wageningen, The

11 Netherlands

12 2- Department of Molecular Phytomedicine, INRES, University of Bonn, Bonn, Germany

13 3- Laboratory of Virology, Wageningen University and Research, Wageningen, The

14 Netherlands

15 4- Department of Bioinformatics and Structural Biochemistry, Institute of Biochemistry of the

16 Romanian Academy, Bucharest, Romania

17

18 **Author's contributions:**

19 A.D-G, M.J.M, H.O., J.R., S.S.P., A.E., F.G., A.G. and G.S. designed the experiments. A.D-G.,

20 M.G.S, H.O., M.J.M, E.C.M., S.S.P., R.P. and S.M-R. conducted the experiments. A.D-G, M.G.S.,

21 J.P., M.H., E.C.M, A.E., F.G., A.J.P., A.G. and G.S, analysed the experiments. A.D-G., M.G.S., G.S.

22 and A.G. drafted the manuscript. All authors revised and agreed to the manuscript

23

24

25 **Corresponding author**: aska.goverse@wur.nl

26

27 **Significance statement**:

28 Here we show that a pathogen effector can target SIZ1, a key protein involved in regulating

29 several aspects of plant biology, most likely to manipulate the SUMOylation of host proteins

30 for successful infection of plants.

31

32 **Running title**: SIZ1 is a nematode effector target involved in plant parasitism

33

34 **Conflict of Interest Statement**: The authors declare no conflict of interest

Abstract

Soil-borne cyst nematodes are obligatory sedentary parasites that cause severe losses to cultivation of major crops such as potato and soybean. Cyst nematodes establish specialised permanent feeding sites within the roots of their host by manipulating plant morphology and physiology through secreted effectors. Here we identified host targets of effector GpRbp-1 and studied their roles in plant-nematode interactions. GpRbp-1 was found to interact in yeast and *in planta* with the potato and Arabidopsis homologues of Siz/PIAS-type E3 SUMO ligase SIZ1. Our results show that a pathogen effector targets the master regulator SIZ1 in plant cells, which has not been demonstrated earlier to our knowledge. The interaction of GpRbp-1 and SIZ1 localizes to the plant nucleus, suggesting that the nuclear functions of SIZ1 as regulator of plant immunity and physiology may be modulated by GpRbp-1. Furthermore, nematode infection assays and transcriptomic profiling indicate that SIZ1 is required for susceptibility to cyst nematodes. So, these data indicate that E3 SUMO ligases may play an important role in plant-nematode interactions. Based on the prediction of SUMO acceptor and interaction sites in GpRbp-1, a model is proposed in which the effector may recruit SIZ1 to be SUMOylated for full functionality in host cells.

Keywords

Cyst nematodes, effectors, GpRbp-1, SUMOylation, SIZ1, stress-responses

Introduction

Plant parasitic nematodes are small round worms that infect the underground parts of their plant hosts. In agricultural settings, nematode infections cause yearly losses in the order of $157 billion (Abad *et al.*, 2008) and it is expected that the rate of nematode infections will increase due to a warmer global climate (Bebber *et al.*, 2013). Cyst nematodes are sedentary endoparasites that penetrate and invade the roots of several major food crops from the Solanaceae family as well as cereals, soybean and sugar beet. Cyst nematodes persist in the soil in recalcitrant cysts that contain hundreds of eggs. In the presence of a host plant, infective juveniles (pre-parasitic J2) hatch from the eggs and penetrate the roots by means of an oral needle-like protractible structure, the stylet. Upon penetration, parasitic-J2 migrate intracellularly in the root until they find a suitable cell for establishment of a permanent feeding site and become sedentary. The characteristic permanent feeding site of cyst nematodes, a so called syncytium, is the sole nutrient source that sustains the nematode through three subsequent life stages i.e. J3, J4 and adult (Kyndt *et al.*, 2013). Eggs develop inside the body of adult females which eventually die and convert into a hardened cyst.

The interaction with the host plant is vital for the completion of the nematode's life cycle and it is largely mediated by a suite of effectors secreted by the nematode. However, only a limited set of effectors has been functionally characterised thus far (Juvale & Baum, 2018). Effectors are produced in two oesophageal glands and secreted selectively throughout

74   the different life stages of the nematode to play different roles during the infection process
75   (Hussey, 1989). For example, several plant cell wall-degrading enzymes are secreted by
76   nematodes at the onset of parasitism to modify or degrade plant cell walls, thereby facilitating
77   intracellular migration (Reviewed in (Wieczorek *et al.*, 2015)). Also, a number of effectors that
78   mediate reprogramming of the plant cells are required for the initiation, establishment and
79   maintenance of the syncytium (Gheysen & Mitchum, 2011; Mitchum *et al.*, 2013; Quentin *et*
80   *al.*, 2013). At the molecular level, nematode secreted effectors function by modifying,
81   competing with, or mimicking the roles of plant structures, genes or proteins. One strategy is
82   the post-translational regulation of host proteins, either directly or indirectly through their
83   interaction with host targets involved in post-translational modification (PTM) (Juvale &
84   Baum, 2018).

85   Post-translational modifications constitute a powerful tool for functional regulation of
86   proteins in eukaryotic cells (Spoel, 2018; Walsh *et al.*, 2005). These regulatory mechanisms
87   rely most often on reversible modifications of peptides and allow a rapid response to variable
88   environmental cues, without requiring gene synthesis (Spoel, 2018). There are different types
89   of post-translational modifications, including the addition of polypeptides onto specific target
90   proteins. The most widely recognised polypeptide addition is ubiquitination, the attachment
91   of several subunits of ubiquitin to target proteins which often function as a molecular marker
92   for protein degradation (reviewed in (Sadanandom *et al.*, 2012; Smalle & Vierstra, 2004)).
93   More recently, an additional small peptide was described (SUMO; Small Ubiquitin-like
94   Modifier) that bears close structural similarities to ubiquitin and can also be conjugated onto
95   target proteins (Matunis *et al.*, 1998). Opposite to ubiquitination, SUMOylation (addition of
96   SUMO) results in variable cellular fates for the target protein. For instance, SUMOylation can
97   alter the subcellular localization, the enzymatic activity or the protein-interaction properties
98   of a target protein (Kurepa *et al.*, 2003; van den Burg *et al.*, 2010; Augustine & Vierstra, 2018;
99   Verma *et al.*, 2018).

100   The cellular machinery for SUMOylation is largely conserved among eukaryotes, and
101   in plants it is best characterised by studies in the model plant *Arabidopsis thaliana*. Four SUMO
102   isoforms SUMO 1/2/3/5 from *A. thaliana* are shown to be functional, with SUMO1 and 2 as
103   the prevalent isoforms serving as substrate for SUMOylation (Kurepa *et al.*, 2003; van den
104   Burg *et al.*, 2010). SUMOylation of target substrates is catalysed by a chain of reactions similar
105   to that of ubiquitination (Kurepa *et al.*, 2003; van den Burg *et al.*, 2010). First, the precursor
106   of SUMO is matured by Ubiquitin-Like Proteases (ULPs) and it is then activated by
107   heterodimeric E1-activating enzymes composed by subunit SAE2 and either SAE1a or SAE1b
108   subunits. The activation of SUMO results in its attachment to the E2 SUMO conjugating
109   enzyme SCE1, which then catalyses the conjugation of SUMO onto an acceptor lysine
110   commonly within the motif ΨKxE in the target protein (Rodriguez *et al.*, 2001). Two E3 ligases,
111   SIZ1 and HYP2 seem to act as enhancers of the activity of the E2 conjugating enzyme (Ishida
112   *et al.*, 2012). Finally, SUMOylation can be reversed by an isopeptidase activity of the SUMO-
113   activating ULPs (Yates *et al.*, 2016).

114   A large amount of evidence places SUMOylation at the nexus of plant responses to
115 (a)biotic stress (Elrouby *et al.*, 2013; Miller *et al.*, 2013). For instance, the abundance of SUMO
116 conjugates increases when plants are subjected to heat shock or chemical exposure, including
117 hydrogen peroxide, copper, and ethanol (Chen *et al.*, 2011; Kurepa *et al.*, 2003). Additionally,
118 Arabidopsis mutants of the different components of the SUMO machinery often display
119 phenotypes defective in tolerance to abiotic stress or pathogen attack (Ishida *et al.*, 2012;
120 Kurepa *et al.*, 2003; Lee *et al.*, 2006; van den Burg *et al.*, 2010). In particular, the knock-out
121 mutant of the SUMO E3 ligase SIZ1 has a strong pleiotropic phenotype, indicating that SIZ1
122 plays a prominent role as regulator in the response to several different types of environmental
123 stresses (Lee *et al.*, 2006). In biotic stress, SIZ1 has been shown to be a negative regulator of
124 salicylic acid-mediated defence, i.e. the *siz1-2* knock-out mutant shows increased resistance
125 to infection by *Pseudomonas syringae* pv. *tomato* (Lee *et al.*, 2006). Due to its prominent role
126 as a negative regulator of plant immunity, SIZ1 would be a valuable target for pathogen
127 effectors to modulate plant immunity for successful infection of their host. However, no
128 evidence is provided for this hypothesis yet.

129   The nematode effector GpRbp-1 belongs to the highly expanded family of SPRYSEC
130 proteins of the potato cyst nematodes *Globodera pallida* and *G. rostochiensis* (Diaz-Granados
131 *et al.*, 2016; Jones *et al.*, 2009; Mei *et al.*, 2015; Rehman *et al.*, 2009). SPRYSEC effectors
132 contain an N-terminal signal peptide for secretion and a C-terminal SPRY domain. The N-
133 terminal signal peptide suggests that SPRYSEC effectors are delivered to the plant cell where
134 they can interact with host proteins. The C-terminal domain, in turn, is proposed to act as a
135 binding platform to mediate interaction with plant target proteins (Diaz-Granados *et al.*,
136 2016). GpRbp-1 is predominantly expressed during the early parasitic stages of nematode
137 infection, which suggests that it plays a role in early parasitism during the initiation and/or
138 establishment of syncytia (Blanchard *et al.*, 2005). A role of GpRbp-1 in nematode virulence is
139 further supported by signatures of positive selection on GpRpb-1 variants from field
140 populations of *G. pallida* (Carpentier *et al.*, 2012). The diversification of this effector family is
141 probably due to specific recognition of certain members by the plant immune system, as
142 shown for the potato immune receptor Gpa2. This receptor recognises specific variants of
143 GpRbp-1 and confers resistance to particular populations of *G. pallida* in the field harbouring
144 the corresponding effector variant (Sacco *et al.*, 2009).

145   To elucidate the role of GpRbp-1 in virulence of *G. pallida*, we aimed to characterize
146 its molecular targets in cells of host plants. We used a combination of protein affinity assays
147 to show that the nematode effector GpRbp-1 interacts specifically in yeast and *in planta* with
148 the SP-RING finger domain of a potato Siz1/PIAS SUMO E3 ligase (StSIZ1). Furthermore, we
149 could demonstrate that this interaction occurs in the nucleus of the plant cell. Similarly,
150 GpRBP-1 was able to interact with AtSIZ1, which prompted us to test the role of SIZ1 in cyst
151 nematode infection by using the *Arabidopsis* mutant *siz1-2*. Infection of *in vitro* grown plant
152 resulted in fewer adult nematodes developing on the roots, consistent with the role of SIZ1 as

153 a negative regulator of basal plant defence to biotrophic pathogens (Lee *et al.*, 2006).
154 Additional evidence was obtained by a comparative RNAseq analysis, which shows that the
155 reduction of nematode susceptibility in *siz1-2* plants is likely due to the activation of defence-
156 related pathways by the *siz1-2* mutation. So, here we show that an effector from a plant
157 pathogen targets the master regulator SIZ1 to promote disease. Moreover, this study provides
158 evidence for a functional role of SIZ1-mediated SUMOylation in nematode parasitism of plant
159 roots. From our data, a picture emerges in which cyst nematodes target SIZ1 in the nucleus to
160 modulate their host through post-translation modifications. To conclude, possible
161 implications on the modulation of SUMOylation (or SIZ1) in plant cells by cyst nematodes are
162 also discussed.

163

164 **Results**

165

166 **GpRbp-1 interacts in yeast with a fragment of SUMO E3 ligase SIZ1 from potato**
167 To find plant interactors of Gp-Rbp-1 we performed a yeast two-hybrid screen of a cDNA
168 library obtained from potato (SH) roots infected with the potato cyst nematode species *G.*
169 *pallida.* We screened a library of $3,85\times10^6$ clones using a variant of GbRbp-1 from field
170 population Rookmaker (GpRbp-1_Rook-1) as bait. Five yeast clones containing cDNA
171 sequences of 858 - 976bp with identities ranging from 97.5 to 100% were found to interact
172 with bait protein GpRbp-1. To identify the candidate plant target that these clones correspond
173 to, we compared the sequences of all fragments against the UniProtKB/Swiss-Prot non-
174 redundant database using the BLASTX algorithm. All clones showed the highest sequence
175 similarity to *Arabidopsis thaliana* E3-SUMO ligase SIZ1 (e-values 2.11×10^{-42} to 9.6×10^{-116})
176 (**Suppl. Table 1**). Among the five yeast clones, there were two pairs with 100% identical
177 sequences within each pair (StSIZfrag10 and StSIZ1frag14; StSIZ1frag49 and StSIZ1frag83). One
178 additional clone contained a fragment that was 87% the length of the fragment contained in
179 the identical clones (StSIZ1frag06). Sequence alignment showed that the clones localized to
180 the C-terminal half of SIZ1 containing a predicted SP-RING finger domain (**Fig. 1; Suppl. Fig. 1**).

181 In Arabidopsis, the *SIZ1* gene encodes four protein domains, an N-terminal SAP domain
182 (Scaffold attachment factors SAF-A/B, Acinus, PIAS), PHD (Plant Homeodomain), a PIIT
183 (proline-isoleucine-isoleucine-threonine) motif, and a SP-RING (SIZ/PIAS-REALLY INTERESTING
184 NEW GENE). Additionally, two SUMO Interacting Motif (SIM) domains were encoded by *AtSIZ1*
185 (Miura *et al.*, 2005) (**Fig. 1**). Finally, AtSIZ1 also contained a nuclear localisation sequence (NLS)
186 in the C-terminal domain of the protein (**Fig. 1**). We compared the coding and peptide
187 sequences of SIZ1 from *Arabidopsis* and potato to investigate their similarity. The full-length
188 coding sequence for *StSIZ1* was obtained from the non-redundant nucleotide database of
189 GenBank (XM_006340080.2). At the nucleotide level, *AtSIZ1* and *StSIZ* shared ~60% identity
190 and at the protein level they shared ~62% identity (**Suppl. Fig. 1**). It should be noted that
191 StSIZ1frag14 and StSIZ1frag83 were 97% identical to StSIZ1, and differences were likely due to

192   the differences in potato genotype used (**Fig. 1B, Suppl. Fig. 1**). Additionally, we investigated
193   the number of copies of *StSIZ1* present in the genome sequence of the doubled monoploid
194   potato genotype DM. To this end, we probed the PGSC *S. tuberosum* group Phureja DM1-3
195   transcripts v3.4 database from the Potato Genomics resource of Michigan University (Hirsch
196   *et al.*, 2014) with a BLASTN algorithm, using AtSIZ as query. Two transcripts
197   (PGSC0003DMT400020963 and PGSC0003DMT400020962; hereafter named 0963 and 0962,
198   respectively) were found corresponding to the same locus in chromosome 11
199   (PGSC0003DMG400008114), with only transcript PGSC0003DMT400020962 considered to be
200   the representative transcript for the locus (Hirsch *et al.*, 2014). Transcript 0963 is 2396bp long,
201   whereas the GenBank StSIZ1 transcript is 3293bp long. An alignment of the protein products
202   for each transcript shows that the peptide encoded by transcript 0962 (StSIZ SpudDB) shares
203   98% identity to the StSIZ1 GenBank peptide and encompasses the C-terminal half of SIZ1
204   protein. These results suggest that StSIZ1 is encoded by a single gene residing on chromosome
205   11 of the DM potato genotype.

206

207   **GpRbp-1 interacts with full length StSIZ1 *in planta***
208   To independently confirm the interaction *in planta*, we used epitope-based co-
209   immunoprecipitation assays. We selected fragments StSIZ1frag14 and StSIZ1frag83 which
210   share a 97% nucleotide identity, differing in ~20 SNPs and 19 nucleotides in length (**Suppl.
211   Table 1**). StSIZ1frag06 shares 100% identity with StSIZ1frag14 and StSIZ1frag83 (**Suppl. Table
212   1**) and was therefore not used to confirm the interaction *in planta*. GpRbp-1 with an N-
213   terminal Myc-GFP tag (Myc-GFP-Rbp1) was co-expressed with the N-terminally HA-tagged
214   fragments StSIZ1frag14 and StSIZ1frag83 (HA-StSIZ1frag14, HA-StSIZ1frag83) by
215   *Agrobacterium tumefaciens* infiltration in *N. benthamiana* leaves. HA-StSIZ1frag14 and HA-
216   StSIZ1frag83 were specifically co-immunoprecipitated by Myc-GFP-Rbp1 and not by Myc-GFP
217   (negative control) captured by magnetic anti-Myc beads (**Fig. 2A**). Therefore, we concluded
218   that GpRbp-1 interacts *in planta* with two fragments corresponding to a sub-region of the SP-
219   RING finger domain of SIZ1 from potato. It is worth noting that after co-immunoprecipitation
220   StSIZ1frag14 and StSIZ1frag83 were detected on western blots as bands migrating
221   approximately 100 KDa higher than the respective bands for the input. This suggests that a
222   complex comprising other peptides may be pulled-down by GpRbp-1.

223   To confirm if GpRbp-1 also interacts with full-length SIZ1 from potato, we performed
224   co-immunoprecipitation assays. First, full-length StSIZ1 was obtained by gene synthesis based
225   on the predicted sequence for SIZ1 from potato transcript variant X2 (GenBank code
226   XM_015314510.1 / SpudDb PGSC0003DMT400020962). N-terminally tagged GpRbp-1 (Myc-
227   GFp-Rbp1) was co-expressed with full-length StSIZ1 with an HA-tag (HA-StSIZ1) in *N.
228   benthamiana* leaves by agro-infiltration. Myc-GFP-Rbp1 captured by magnetic anti-Myc
229   beads, co-immunoprecipitated HA-StSIZ1 (**Fig. 2B**). A Myc-GFP (negative control) did not co-
230   immunoprecipitate HA-StSIZ1, indicating a specific interaction of GpRbp-1 with StSIZ1. These
231   results showed that GpRbp-1 was able to interact specifically with StSIZ1 *in planta*.

232

StSIZ1 and GpRpb-1 co-localize when expressed *in planta*

234 A C-terminal nuclear localization signal (NLS) was predicted in StSIZ1. Additionally, SIZ1 from
235 Arabidopsis is exclusively located within the nucleus of cells (Miura, 2005). Therefore, we
236 investigated the localization of StSIZ1 *in planta* by expressing N-terminally GFP-tagged StSIZ1
237 by transient transformation in *N. benthamiana* leaves. The localization of GFP-StSIZ1 followed
238 a similar nuclear localization as previously reported for AtSIZ1 and the tomato homologue
239 SlSIZ1 (**Fig. 3**) (Lee *et al.*, 2006; Zhang *et al.*, 2017). Moreover, we observed that the GFP
240 fluorescent signal was uneven throughout the nucleus, with stronger emission in discrete
241 globules within the nucleus, which was also consistent with the localization reported for
242 AtSIZ1. Additionally, StSIZ1 was co-expressed with GpRbp-1 to evaluate their subcellular
243 localization *in vivo* by confocal laser scanning microscopy (CLSM). Co-transformed mCherry-
244 labelled GpRpb-1 (mCh-Rbp1) and GFP-labelled StSIZ1 (GFP-StSIZ1) in *N. benthamiana* leaves
245 were evaluated. When expressed in combination with free GFP, GpRbp-1 was consistently
246 distributed between the nucleus and the cytoplasm as established previously (Jones *et al.*,
247 2009). GFP-StSIZ1 localized to the nucleus with higher expression levels in defined nuclear foci
248 when co-expressed with free mCherry. When co-expressed, GFP-StSIZ1 and mCh-Rbp1 co-
249 localized to the nucleus of transformed cells, suggesting that an interaction occurs in the
250 nucleus. Moreover, we concluded that the subcellular localization of GpRbp-1 or StSIZ1 was
251 not altered upon co-infiltration and apparently, is not affected by their complex formation.
252 The fluorescent tags were fused to the N-terminus of GpRbp-1 and StSIZ1 to simulate as
253 closely as possible the configuration of the proteins in the interaction studies. There, the yeast
254 binding domains or epitope tags were also fused to the N-terminal regions of the CDS of the
255 interactors.

256

GpRbp-1 interacts with StSIZ1 and AtSIZ in the plant cell nucleus

258 To test if GpRbp-1 indeed interacts with StSIZ1 in the nuclear compartment we performed a
259 bimolecular complementation assay (BiFC). For BiFC, the N-terminal half of the super cyan
260 fluorescent protein SCF3A was fused to GpRbp-1 (pN:Rbp1) and the C-terminal half of SCFP3A
261 was fused to StSIZ1 (pC:StSIZ1). The fluorescent fusions were transiently expressed in *N.*
262 *benthamiana* by agroinfiltration. pN:Rbp1 was co-infiltrated with the viral protein NSs fused
263 to the C-terminal half of protein SCFP3A (pC:NSs) and pC:StSIZ1 was co-infiltrated with β-
264 glucuronidase fused to the N-terminus of SCFP3A (pN:GUS) as negative controls. The
265 characteristic emission of SCFP3A was only reconstituted when pN:Rbp1 and pC:StSIZ1 were
266 co-expressed (**Fig. 4**). There was no reconstitution of the fluorescent signal of CFP when
267 pN:Rbp1 was co-expressed with pC:NSs, neither by the co-expression of pC:StSIZ1 with
268 pN:GUS. These findings confirmed that GpRbp-1 and full-length StSIZ1 interacted specifically
269 *in planta* (**Fig. 2**; **Suppl. Fig. 1**). Interestingly, the fluorescent signal of CFP was only detected
270 in the nucleus of transformed cells, confirming that GpRpb-1 and StSIZ1 only interact within

271 this cellular compartment. Moreover, the observed granular fluorescent pattern suggests that
272 the interaction between GpRpb-1 and StSIZ1 follows specific substructures within the nuclei.

273 Having confirmed that GpRbp-1 targets StSIZ1 in the nucleus, we wondered if GpRbp-
274 1 was also able to interact with distant homologues of SIZ1 from plant species which were also
275 infected by cyst nematodes like the model species Arabidopsis. To investigate if GpRbp-1 was
276 able to interact with AtSIZ1, we performed similar BiFC assays. N-terminally tagged AtSIZ with
277 the C-terminal half of SCF3A (pC:AtSIZ1) was transiently co-expressed with pN:Rbp-1 in leaves
278 of *N. benthamiana*. The fluorescent signal characteristic of SCF3A was reconstituted when
279 pN:Rbp-1 was co-expressed with pC:AtSIZ1, but not when co-expressed with the negative
280 control pC:NSs or pN:GUS in case of pC:AtSIZ (**Fig. 4**). The re-constituted signal indicating the
281 interaction of pN:Rbp-1 and pC:AtSIZ1 was only visible in the nucleus of co-transformed cells.
282 This shows that effector GpRbp-1 is also able to interact with AtSIZ1 *in planta* and that this
283 interaction was limited to the nuclear cavity.

284

285 **SUMO-E3 ligase SIZ1 is involved in cyst nematode infection of *A. thaliana***
286 Based on the selective interaction of GpRbp-1 with both StSIZ1 and AtSIZ1, the role of SIZ1 in
287 nematode infection was further tested *A. thaliana* and the beet cyst nematode *Heterodera*
288 *schachtii* as a model system. First, we investigated the expression of *AtSIZ1* during cyst
289 nematode infection. We measured the expression of *AtSIZ1* by quantitative RT-PCR in whole-
290 roots of *H. schachtii* or mock-inoculated plants (Columbia-0) at 2, 4, 10, and 14 days post-
291 inoculation (dpi). No differential expression of the *AtSIZ1* transcript upon nematode infection
292 was detected (**Suppl. Fig. 4**). From these data, we concluded that the *AtSIZ1* gene expression
293 is not differentially regulated during cyst nematode infection which is consistent with a
294 regulatory role in post-translational modification of proteins required for nematode
295 parasitism.

296 To investigate if SIZ1 was involved in nematode infection we challenged *in vitro*-grown
297 *siz1-2* knockout *A. thaliana* mutant with *H. schachtii*. These mutant lines carry an independent
298 homozygous T-DNA insertion at different sites of exon 16 of the *AtSIZ1* gene resulting in a
299 knock-out of SIZ1 (Lee *et al.*, 2006; Miura *et al.*, 2005). The homozygosity of the T-DNA
300 insertion was verified using PCR primers designed with the iSect tool from the SALK Institute
301 Genomics Analysis Laboratory (**Suppl. Table 6**). To examine the importance of AtSIZ1, the total
302 number of nematodes infecting the roots of the mutant and wild-type control (Col-0) were
303 counted at 14 dpi. Furthermore, we discriminated between adult female and male
304 nematodes, as this indicates the nutritional quality of the established infection sites (Anjam
305 *et al.*, 2018; Trudgill, 1967). We observed a significant decrease of 36% (one-way ANOVA,
306 p<0.001) in the total number of nematodes infecting the roots of *siz1-2* mutant as compared
307 to the wild-type plants, respectively (**Fig. 5**; **Suppl. Fig. 5**). In addition, the number of female
308 nematodes present in the roots of *siz1-2* was reduced by 49% in the mutant as compared to
309 wild-type plants (one-way ANOVA, p<0.001). A similar effect was observed for the number of
310 males, where a decrease of 29% in *siz1-2* plants as compared to the wild-type was found (one-

311 way ANOVA, p<0.001) (**Suppl. Fig. 5**). Under *in vitro* growth conditions we did not observe an
312 aberrant growth phenotype of the roots in the *siz1-2* seedlings, which was consistent with
313 previous reports (Castro *et al.*, 2015; Catala *et al.*, 2007; Miura *et al.*, 2011). Hence, the
314 reduction in susceptibility could be attributed to the *siz1-2* mutation and not to differences in
315 the mutant root systems. Therefore, we concluded that SIZ1 plays a role in the susceptibility
316 of *Arabidopsis* to infection by cyst nematodes.

317   Additional evidence was obtained by investigating the effect of SIZ1 on the size of the
318 feeding site and growth of female nematodes infecting the roots of Arabidopsis. To this end,
319 we measured the surface area of syncytia and females visible in the roots of *siz1-2* and wild-
320 type Arabidopsis after two weeks of infection. The size of the syncytia induced by *H. schachtii*
321 in *siz1-2* was 20% smaller as compared to the wild-type (one-way ANOVA, p<0.001) (**Fig. 5**).
322 The size of the females established in *siz1-2* plants was not significantly different as compared
323 to those developing on wild-type Arabidopsis plants (one-way ANOVA, p=0.335) (**Fig. 5**).
324 Together, these results suggest that SIZ1 may not only contribute to the control of the overall
325 infection rate, but might also influence the expansion of the permanent feeding sites of cyst
326 nematodes in Arabidopsis.

327

328 **AtSIZ1 may contribute to plant defence to cyst nematodes**

329 To further understand the role of SIZ1 during nematode interactions we performed a whole
330 transcriptome analysis of *siz1-2* and wild-type Arabidopsis roots infected with beet cyst
331 nematodes. To uncouple the effects of a mutated genotype and infection, we isolated whole
332 root RNA from mock-inoculated and cyst nematode inoculated plants for both *siz1-2* and the
333 wild-type plants, 7 days after inoculation (n = 3 replicates for each sample). We observed the
334 overall expression of 13,114 genes in all 12 samples, and principal component analysis (PCA)
335 showed a clear distinction between the *siz1-2* mutant and wild-type (first principal
336 component, 27.1% of variance), and non-infected versus *H. schachtii* infected (second
337 principal component, 13.4% of variance) (**Fig. 6**) as expected. Interestingly, the non-infected
338 *siz1-2* and infected *siz1-2* samples cluster closer together on the 2nd principal component axis
339 than the non-infected and infected wild-type. This clustering indicates that *siz1-2* plants show
340 less difference upon infection, the impact of the cyst nematodes on the transcriptome is
341 smaller in the *SIZ1* mutant than in the wild-type (**Fig. 6**). The infection-like transcriptional
342 profile of *siz1-2* is likely reflecting the auto-immune phenotype previously reported for *siz1*-2
343 and the role of *SIZ1* as negative regulator of SA-mediated stress responses (Lee *et al.*, 2006).

344   To uncover which genes contributed to the separation of the samples in the PCA, we
345 used a linear model to find 171 genes contributing to the difference between *siz1-2* and wild-
346 type, 29 genes between non-infected and *H. schachtii* infected plants, and 9 genes between
347 *siz1-2* and wild-type upon infection (interaction) (linear model, p < 0.0001; $FDR_{genotype}$ = 0.011,
348 $FDR_{infection}$ = 0.064, $FDR_{interaction}$ = 0.131; **Fig. 6**; **Suppl. Table 3**; **Suppl. Table 4**). To examine the
349 hypothesis that nematodes manipulate a specific molecular pathway through SIZ1, we

350   evaluated the gene ontology (GO) annotations of the 9 genes that are differentially regulated
351   by the combination of mutant genotype and infection (**Suppl. Table 5**). Genes involved in
352   control of the cell cycle (e.g. CYC B2;2), defence (e.g. BAP2) and protein transport (e.g. SLY1)
353   were found in this differentially regulated group. Nevertheless, the small number of genes
354   affected by the combination of the *siz1-2* mutation and the nematode infection (interaction)
355   limits further interpretation of the molecular processes or pathways that nematodes may
356   manipulate through SIZ1. In addition, the strong transcriptional differences between wild-type
357   and *siz1-2* plants prior to infection, supported the notion that a mutation in SIZ1 induces
358   drastic changes in the plant, even more so than infection with cyst nematodes.

359   To understand further the specific genes that were affected by the *siz1-2* mutation, we
360   performed a gene-enrichment analysis. Thirty gene ontology (GO) terms are significantly
361   upregulated in the *siz1-2* mutant, including "located in cell wall", "involved in abiotic or biotic
362   stimulus", "cellular response to ethylene stimulus", and "functions in carbohydrate binding"
363   (**Suppl. Table 5**). In contrast, seven gene ontology categories are significantly upregulated in
364   the wild-type, including "functions in sequence-specific DNA binding", "located in extracellular
365   region", "involved in response to cold", and "functions in sequence-specific DNA binding"
366   (**Suppl. Table 5**). It is worth noting that the GO term most significantly upregulated in *siz1-2*
367   plants is "involved in cellular response to ethylene stimulus". Likewise, the GO term most
368   significantly upregulated in wild-type plants is "functions in sequence-specific DNA binding"
369   (**Suppl. Table 5**). These findings further support the existence of an "infection-like"
370   transcriptional state of the *siz1-2* plants as detected with the PCA analysis due to constitutive
371   activation of defence pathways as previously reported.

372

Discussion
374   GpRbp-1 is an effector secreted by the potato cyst nematode *G. pallida* during the onset of
375   parasitism, presumably to promote nematode virulence. To characterise the virulence role of
376   this effector we aimed to identify the host proteins targeted by GpRbp-1. We found that
377   GpRbp-1 interacts specifically in yeast and *in planta* with the potato homologue of the SUMO
378   E3 ligase SIZ1. Furthermore, evidence from live cell imaging indicates that this interaction was
379   limited to the nucleus of the cell, where GpRbp-1 co-localizes with StSIZ1. In addition, we
380   evaluated the role of SIZ1 during nematode parasitism in the Arabidopsis - *H. schachtii* model
381   system. *In vitro* infection studies in the Arabidopsis *siz1-2* mutant show that SIZ1 contributes
382   to infection by cyst nematodes presumably as a negative regulator of plant defence. These
383   results suggest that GpRbp-1 may target SIZ1 to repress plant immunity. This provides
384   therefore evidence for the targeting of the master regulator SIZ1 by a pathogen effector to
385   promote its virulence.

386   Likewise, the involvement of SUMOylation in plant-nematode interactions had not
387   been described previously to the best of our knowledge. In contrast, SUMOylation has been
388   shown to play a role in virulence of other plant pathogens. For instance, proteins from the
389   SUMO machinery are transcriptionally regulated during infection by *Phytophthora infestans*

390 in potato (Colignon *et al.*, 2017). Also, interaction of replication protein AL1 from the
391 geminivirus Tomato Golden Mosaic Virus and the SUMO E2-conjugating enzyme SCE1, is
392 required for viral infection in *N. benthamiana* (Castillo *et al.*, 2004; Sanchez-Duran *et al.*,
393 2011). Furthermore, the effector XopD from *Xanthomonas euvesicatoria* has SUMO-protease
394 activity, and catalyses the removal of SUMO from the tomato transcription factor SlERF4 to
395 supress ethylene-mediated immune responses (Kim *et al.*, 2013).

396   The reduced susceptibility of *A. thaliana* mutants *siz1-2* to cyst nematode infection
397 (**Fig. 5**) likely reflects the role of SIZ1 as a negative regulator of plant immunity (Gou *et al.*,
398 2017; Hammoudi *et al.*, 2018; Lee *et al.*, 2006; Niu *et al.*, 2019). The *Arabidopsis siz1-2* mutant
399 is characterised by a dwarf phenotype associated to increased levels of salicylic acid (SA) (Lee
400 *et al.*, 2006). This increased SA production in *siz1-2* is also associated to an upregulation of
401 pathogenesis-related (PR) genes such as *PR1* and *PR5* (Lee *et al.*, 2006). Additionally, the
402 mutation in *siz1-2* confers resistance to the bacterial pathogen *Pseudomonas syringae* p.v
403 *tomato (Pst)* (Lee *et al.*, 2006). In contrast, the susceptibility of *siz1-2* to the fungal pathogen
404 *Botrytis cinerea* is comparable to that of the wild-type (Lee *et al.*, 2006). Therefore, Lee and
405 co-workers (Lee *et al.*, 2006) proposed that SIZ1 regulates immunity mediated by SA to
406 biotrophic pathogens like *P. syringae,* independent of the jasmonic acid (JA) signalling
407 pathway induced by the necrotrophic pathogen *B. cinerea*. Interestingly, cyst nematodes are
408 also biotrophic pathogens, which trigger local and systemic SA-mediated plant defence
409 responses upon root invasion (Kammerhofer *et al.*, 2015; Lin *et al.*, 2013; Nguyen *et al.*, 2016;
410 Wubben *et al.*, 2008; Youssef *et al.*, 2013). Together, these results suggest that SIZ1 may be
411 required for basal resistance to biotrophic pathogens with different modes of infection above-
412 and belowground.

413   In line with the auto-immune phenotype of the *siz1-2* mutant (Lee *et al.*, 2006), our
414 gene enrichment analysis shows that stress-related genes are differentially regulated in the
415 *siz1-2* mutant in the absence of nematode infection (**Fig. 6; Suppl. Table 4**). It should be noted
416 that we did not find elevated levels of *PR-1* or *PR-5* SA-responsive genes in the roots of *siz1-2*
417 Arabidopsis. This observation may be due to the differences in growth conditions that may
418 repress accumulation of SA or specific events in the SA-responsive pathway, or to different
419 expression patterns of *PR* genes in roots and shoots. In addition, very few genes were
420 differentially regulated in response to the infection of the mutant, suggesting that nematode
421 infection has a relatively minor effect on transcriptional regulation of plant roots, as compared
422 to the mutation alone (**Fig 6; Suppl. Table 4**). Therefore, our RNA-Seq data supports the
423 hypothesis that the auto-immune phenotype of the *siz1-2* mutant underlies the mutant's
424 reduced susceptibility to infection by cyst nematodes. From this, a model can be inferred in
425 which the immune-repressive function of SIZ1 in SA-mediated defence responses is enhanced
426 by nematode effectors leading to an increase in the susceptibility of host plants to cyst
427 nematode infections.

428   In plants, a zinc-finger motif within the SP/RING domain is largely responsible for the
429 nuclear localization of AtSIZ1 as well as the regulatory role of SA accumulation and SA-

430   dependent phenotypes (e.g. dwarfism, resistance to pathogens and thermotolerance)
431   (Cheong *et al.*, 2009). Interestingly, GpRbp1 interacts with a protein fragment comprising this
432   domain of SIZ1, suggesting that it may affect the SUMO E3 ligase activity of SIZ1. Furthermore,
433   the nuclear co-localization and interaction of GpRbp-1 and StSIZ1 seems to follow specific
434   substructures within the nucleus (**Figs. 3 and 4**). This may point at targeting of StSIZ1 by
435   GpRbp-1 to modify or modulate the nuclear activity of StSIZ. In yeast, the RING domain is
436   necessary to recruit the E2-SUMO complex into a complex with its substrate (Yunus and Lima,
437   2009). Hence, targeting of the SP-RING finger domain of SIZ1 by GpRbp-1 most likely
438   compromises these SA-related phenotypes. In turn, the characteristic hypervariable region of
439   GpRbp-1 may function as a binding platform to facilitate the targeting of SIZ1 (Diaz-Granados
440   *et al.*, 2016; Rehman *et al.*, 2009).

441   Additionally, the gene ontology "involved in cellular response to ethylene stimulus"
442   was the enriched category with the highest statistical support. From the differentially
443   regulated genes, LEC1 (lectin-like protein; AT3G15356), FRD3 (Ferric reductase defective 3;
444   AT3G08040), and RBK1 (ROP binding protein kinase; AT5G10520) are grouped in the
445   "response to ethylene stimulus" ontology (**Suppl. Table 4**). LEC1 has been shown to be
446   transcriptionally regulated in response to several stimuli, including the fungal elicitor chitin
447   and mechanical wounding. The response of LEC1 to chitin is also found in ethylene/jasmonate
448   (ET/JA)-insensitive mutants, suggesting that LEC1 is involved in ET/JA-dependent and
449   independent cellular responses (Seoung Hyun *et al.*, 2009). This finding could indicate that,
450   opposite to previous hypotheses (Lee, 2006), SIZ1 may be involved in regulation of the JA
451   defence pathway through modulation of the JA/ET branch (Pieterse *et al.*, 2012). Moreover,
452   in plant-nematode interactions ethylene can act as a modulator of SA-immunity or as a
453   regulator or cytokinin-dependent susceptibility, and these roles are determined by the
454   activation of specific ethylene receptors (Piya *et al.*, 2019). Therefore, it remains to be
455   determined if SIZ1 acts solely as a regulator of SA-mediated plant immunity in plant nematode
456   interactions.

457   SIZ1 may also act as regulator or hormone-dependent metabolic processes that
458   influence susceptibility to nematodes. The decrease in the size of the specialised feeding sites
459   (syncytia) induced by nematodes in *siz1-2* plants points to a role of SIZ1 in expansion of
460   nematode-induced feeding sites (**Fig. 5**). Additionally, the genes differentially regulated by the
461   *siz1-2* mutation in combination with cyst nematode infection may have further roles as
462   regulators of feeding site formation. For example, in addition to ethylene responsiveness,
463   FRD3 is also involved in nutrient homeostasis and iron uptake (Xing *et al.*, 2015). And in turn,
464   RBK1 has been shown to be regulated by pathogen infection (Molendijk *et al.*, 2008), but also
465   to be implicated in auxin-mediated cell expansion (Enders *et al.*, 2017). Both nutrient uptake
466   and cell expansion processes are relevant in the context of nematode feeding sites (reviewed
467   in (Kyndt *et al.*, 2013)).   Finally, SIZ1 represses the characteristic root morphological
468   adaptations to phosphate starvation, through the control of auxin patterning (Miura *et al.*,
469   2011; Miura *et al.*, 2005). Auxin transport and signalling are involved in the proper formation

470 of syncytia, presumably by its role as regulator of plant organogenesis (reviewed in (Gheysen
471 & Mitchum, 2019; Ng *et al.*, 2015)). These findings illustrate how the regulatory network of
472 SIZ1 becomes intricate, with effects on different plant hormones that are implicated in
473 immune responses as well as in cellular modifications related to nematode infection.
474 Ultimately, elucidating the mechanism of action of SIZ1 would require the identification of the
475 molecular targets that are regulated by SIZ1 in plant-nematode interactions. Nevertheless,
476 around 600 proteins are predicted as potential SIZ1-dependent SUMO targets in plants (Rytz
477 *et al.*, 2018). Consequently, a definite mode of action of SIZ1 in plant-nematode interactions
478 will require further dissection through a combination of genetic, biochemical and *in vivo*
479 assays.

480 Preliminary data also provide evidence for a complementary hypothesis where GpRbp-
481 1 may modulate host cellular processes by recruiting the SUMO machinery of the host. Here,
482 we could show that GpRbp-1 interacts in BiFC with other components of the SUMO machinery,
483 namely SUMO1, 3 and 5 (SUM1, SUM3, SUM5) and the E2 conjugating enzyme SCE1 (**Supp.**
484 **Fig. 6**). Interestingly, GpRbp-1 interacts with the SUMOs and SCE1 in the nucleus and
485 cytoplasm, where these proteins localize (**Suppl. Fig. 6**) (Mazur *et al.*, 2019; Xiong & Wang,
486 2013). In yeast and mammals, multi-protein complexes including SUMO, E2 (Ubc9), and E3s
487 (PIAS/Nup358) (Mascle *et al.*, 2013; Reverter & Lima, 2005) are required for SUMOylation and
488 the ensuing transcriptional regulation activities of UBC9 and SUMO1 (Mascle *et al.*, 2013;
489 Reverter & Lima, 2005). Similarly, in *Arabidopsis* SUMO, SCE1 and SIZ1 form a ternary complex
490 that is recruited to nuclear bodies (NBs) where COP1 is SUMOylated to regulate the response
491 of the plant to darkness and temperature (i.e. skoto- and thermo-morphogenesis) (Kim *et al.*,
492 2016; Lin *et al.*, 2016; Mazur *et al.*, 2019; Osterlund *et al.*, 2000; Seo *et al.*, 2003; Yang *et al.*,
493 2005). Conceivably, the virulence role of GpRbp-1 may be exerted through an influence on the
494 SUMO-SCE1-SIZ1 tertiary complex, for example by stabilisation. In support of this notion, our
495 co-immunoprecipitation assays suggest that intermediate compounds present in a larger
496 complex with StSIZ1frag14 and StSIZ1frag83 are co-pulled down specifically by GpRbp-1 (**Fig.**
497 **2**). The nature of the complex co-pulled down along with StSIZfrag14 and StSIZ1frag83 by
498 GpRbp-1 the remains to be established.

499 An alternative explanation is that GpRbp-1-like effectors may recruit the SUMO
500 complex to achieve SUMOylation inside the host cells for full functionality as an effector.
501 Conceivably the SUMOylation of GpRbp-1-like effectors may enhance their stability by
502 competing with ubiquitination (Zheng *et al.*, 2018) or modify their binding patterns (Guo &
503 Sun, 2017; Hansen *et al.*, 2017). This hypothesis is supported by the prediction of consensus
504 SUMO-acceptor (ψKxE) and SUMO-interaction motifs (SIM) in GpRbp-1 (**Suppl. Fig. 7**),
505 indicating that host-mediated SUMOylation may be relevant for its functioning as an effector.
506 Two SIM are predicted in the N-terminal half of GpRbp-1, in one region that is unique to
507 GpRbp-1 and another present in several Rbp and SPRYSEC sequences (Diaz-Granados *et al.*,
508 2016). The first SIM, unique to GpRbp-1 falls within a region with low confidence for
509 modelling, so it is difficult to predict in what region of the GpRbp-1 structure it is located. The

510 second SIM (SIM2) localizes to a β-sheet present in the core of the β-sandwich structure that
511 is predicted for GpRbp-1 (**Suppl. Fig. 7**). In addition, two ψKxE SUMOylation sites are
512 predicted, one inverted in the conserved core of the SPRY domain (ψKxE_inverted) and one
513 in the C-terminus in a motif present only in GpRbp-1 and Rbp-1 from *G. mexicana* (ψKxE_2)
514 (Diaz-Granados *et al.*, 2016) (**Suppl. Fig. 7**). The "conserved" SIM2 and (ψKxE inverted) sites
515 reside in the β-sheet core of GpRbp-1, and most likely form a binding pocket for SUMO,
516 whereas the unique ψKxE_2 site resides in a C-terminal α-loop and is likely exposed to the
517 solvent (**Suppl. Fig. 7**). None of these motifs contain residues reported to be under positive
518 selection in *G. pallida* field populations (Carpentier *et al.*, 2012). In this scenario, the lack of
519 SIZ1 in *siz1-2 Arabidopsis* impedes an efficient functioning of GpRbp-1 homologues from *H.*
520 *schachtii* as a virulence factor. Although the functional homolog of GpRbp-1 of *H. schachtii* is
521 not known, we assume that similar proteins may exist based on the existence of GpRbp-1-like
522 gene transcripts (Fosu-Nyarko *et al.*, 2016) which may exert a similar function in plant
523 parasitism. Moreover, different cyst nematode species share the same mode of parasitism,
524 which results in the formation of typical feeding structures. Therefore, we expect that the
525 underlying molecular mechanisms are conserved among host plant species. This is supported
526 by our observation that GpRbp-1 can also interact with AtSIZ1 (**Fig. 4**), suggesting that SIZ1
527 may be a conserved target of cyst nematodes.

528

Experimental procedures

Yeast two-hybrid – library screen

531 The prey *G. pallida*- infected potato library was generated by Dual Systems Biotech
532 (Switzerland) from grinded roots of potato (*Solanum tuberosum* ssp. *andigena*) genotype SH
533 infected with juveniles of *G. pallida* population Pa3-Rookmaker. Potato plantlets were grown
534 on 16 cm square plates containing B5 medium at 20°C in 16 h light/ 8 hours dark conditions.
535 Two weeks after transplant, plantlets were inoculated with ~200 juveniles. Infected roots
536 were collected at 2, 3, 7, 9, 12 and 14 dpi and grinded in liquid nitrogen before shipping. Poly
537 (A) tailing and total RNA isolation were performed by Dual Systems Biotech (Switzerland) and
538 a cDNA library consisting of $3,85 \times 10^{6}$ clones with an average insert size of 1.13Kb was
539 constructed. The library yeast two-hybrid screen was performed by Dual Systems Biotech
540 (Switzerland) using the DUALhybrid vector system.

541

Cloning

543 For co-immunoprecipitation, the interacting fragments StSIZ1fragDS14 and StSIZ1fragDS83
544 were excised from the pGAD-HA prey vector using NcoI and XhoI restriction sites. The NcoI-
545 XhoI fragment includes the StSIZ1fragDS14 and StSIZ1fragDS83 with an N-terminal
546 hemagglutinin (HA) tag. The NcoI-XhoI fragment was inserted into vector pRAP digested with
547 NcoI and SalI. In the vector and additional four units of N-terminal HA tag are fused to the HA-
548 StSIZ1fragDS14 and HA-StSIZ1fragDS83. The fusion cassette was digested with PacI and AscI

549 and ligated into vector pBIN. In pBIN, the HA-StSIZ1fragDS14 and HA-StSIZ1fragDS83 fusion is
550 under the control of the 35S constitutive promotor. GpRpb-1 version 1 from virulent
551 population Rookmaker (Rook1) was tagged with an N-terminal fusion of 4 units on the c-Myc
552 tag followed by a GFP (Myc4-GFP-GpRbp-1) and transferred by restriction enzyme cloning to
553 the pBINPLUS binary vector (van Engelen *et al.*, 1995). For microscopy studies, the full-length
554 gene of StSIZ1 was obtained by synthetic gene synthesis (GeneArt) (Thermo Fisher Scientific,
555 Waltham, Massachusetts) and cloned to appropriate pGWB vectors (Nakagawa *et al.*, 2007)
556 by Gateway cloning. The mCherry GpRbp-1 construct was generated by restriction cloning in
557 pBINPLUS (van Engelen et al., 1995). BiFC constructs were generated by Gateway cloning to
558 the pDEST-SCYCE(R)^{GW} and pDEST-SCYNE(R)^{GW} vectors (Gehl *et al.*, 2009).

559 The full-length gene of StSIZ1 was obtained by synthetic gene synthesis (GeneArt) using the
560 potato CDS transcript variant X3 (GenBank accession XM_006340080.2) into Gateway-
561 compatible pMA vector. StSIZ1 was synthesized with an additional N-terminal BamHI site and
562 a C-terminal PstI site in order to enable restriction cloning. The internal BamHI and PstI
563 restriction sites were disrupted by introducing silent mutations. The codons were always
564 replaced with ones with similar or higher usage frequency in *Nicotiana benthamiana*
565 *(*Nakamura et al., 20*00)*. Full-length SIZ1 N-terminally tagged with HA or GFP was obtained by
566 gateway cloning to plant-expression vectors pGWB415 and pGWB425 respectively,
567 (Nakagawa *et al.*, 2007) for interaction and localization studies.

568 For bimolecular fluorescence complementation (BiFC), GpRbp1 was amplified by PCR and
569 cloned into pDONR207 by a BP reaction, following the manufacturer's instructions
570 (Invitrogen). Expression clones of GpRbp1 were obtained by LR recombination into pDEST-
571 SCYCE(R)^{GW} BiFC vector (Gehl *et al.*, 2009). Similarly, expression clones of full-length SIZ1
572 (StSIZ1) were recombined by LR recombination (Invitrogen) into pDEST-SCYNE(R)^{GW} BiFC
573 vector following the manufacturer's instructions (Gehl *et al.*, 2009). cDNA of SCE1, SUMO1,
574 SUMO3 and SUMO5 from Arabidopsis was obtained from total RNA extracted with TRIzol
575 reagent (Thermofisher), followed by first-strand cDNA synthesis using M-MLV reverse
576 transcriptase (Promega) and random hexamers (Roche) according to the manufacturer's
577 protocols. Primer pairs containing attB1 and attB2 recombination sites (**Suppl. Table 6**), were
578 used to amplify the coding sequences of SCE1, SUMO1, SUMO3 and SUMO5, respectively. The
579 resulting PCR amplicons were recombined with the Gateway vector pDONR207
580 (Thermofisher) by BP reaction, following the manufacturer's instructions. Subsequently,
581 expression clones were generated by LR recombination into the pDEST-SCYNE(R)^{GW} BiFC
582 vector following the manufacturer's instructions (Gehl *et al.*, 2009).

583

584 **Expression and detection of recombinant proteins**

585 All proteins were co-expressed by Agrobaterium-mediated transient transformation of
586 *Nicotiana benthamina* leaves. All co-expression assays are done together with the silencing
587 supressor p19, with a final concentration of OD$_{600}$=0.5. Total protein extracts were prepared
588 by grinding leaf material in protein extraction buffer. For co-IP, pull-downs were performed

589   using μMACS anti-c-MYC or anti-HA paramagnetic beads (Miltenyi, Bergisch Gladbach,
590   Germany). Proteins were separated by SDS-PAGE on NuPage 12% Bis-Tris gels (Invitrogen,
591   Carlsbad, California) and blotted to 0.45μm polyvinylidene difluoride membrane (Thermo
592   Fisher Scientific). Immunodetection was performed with corresponding horseradish
593   peroxidase-conjugated antibodies. Confocal microscopy was performed on *N. benthamiana*
594   epidermal cells using a Zeiss LSM 510 confocal microscope (Carl-Zeiss, Oberkochen, Germany)
595   with a 40X, 1.2 numerical aperture water-corrected objective.

596

597   **Confocal microscopy**
598   *N. benthamiana* epidermal cells were examined using a Zeiss LSM 510 confocal microscope
599   (Carl-Zeiss) with a 40X 1.2 numerical aperture water-corrected objective. For co-localization
600   studies the argon laser was used to excite at 488 nm for GFP and chlorophyll, and the HeNe
601   laser at 543nm to excite mCherry. GFP and chlorophyll emission were detected through a
602   band-pass filter of 505 to 530nm and through a 650nm long-pass filter, respectively. mCherry
603   emission was detected through a band-pass filter of 600 to 650nm. For BiFC the argon laser
604   was used to excite at 458 nm for SCFP3A. SCFP3A emission was detected through a band-pass
605   filter of 470nm to 500nm and chlorophyll emission was detected through a 615nm long-pass
606   filter. We also used a CFP marker to calibrate the fluorescence excitation and emission for CFP.

607

608   **Plant material and nematode infection**
609   Seeds of the homozygous *siz1-2* were kindly provided by Dr. H. van den Burg (Laboratory for
610   Phytopathology, University of Amsterdam, the Netherlands). Col-0 N60000 wildtype seeds
611   were obtained from the SALK homozygote T-DNA collection (Alonso et al., 2003).–For
612   nematode infection, seeds were vapour sterilized and sown in modified KNOP medium
613   (Sijmons *et al.*, 1991) and grown at 25°C under a 16-h-light/8-h-dark cycle. 10 day-old
614   seedlings were inoculated with 60-70 surface-sterilized *H. schachtii* infective juveniles. After 2
615   weeks of infection, the amount of nematodes present in the roots of Arabidopsis plants were
616   counted visually and the size of females and syncytia were determined as described previously
617   (Siddique *et al.*, 2014). Statistical differences were estimated by one-way ANOVA (α=0,05),
618   using the weighted-inverse variants to combine data from 4 biological replicates.

619

620   **RNA sequencing**
621   *Total RNA extraction*
622   Seeds of *siz1-2* and Col-0 wild-type (N60000) were vapour sterilized and sown in modified
623   KNOP medium (Sijmons *et al.*, 1991) in 6-well cell culture plates (Greiner Bio-one). Seedlings
624   were grown at 21°C under a 16-h/8-h light/dark regime. Two-week old seedlings were infected
625   with approximately 180 surface-sterilized *H. schachtii* juveniles. One week after inoculation
626   the complete root systems of ~18 *siz1-2* and Col-0 plantlets were harvested and snap-frozen.
627   Root tissue was ground in liquid nitrogen and total RNA was extracted with the Maxwell® 16

628   LEV plant RNA kit (Promega) in the Maxwell 16 AS2000 instrument (Promega), following the
629   manufacturer's instructions. Three biological replicates of ~18 plants/sample per condition
630   were generated.

631   *Count derivation and normalization*

632   Quality checking, removal of adapter sequences, genome mapping and count derivation was
633   performed by a custom-written pipeline. Briefly, read quality was assessed using FASTQC
634   v0.11.5 (Andrews, 2014). Overrepresented adapter sequences, base pairs with a Q-value
635   lower than fifteen in the 5' or 3' and reads shorter than 20bp were removed with cutadapt
636   v1.16 (Martin, 2011). Reads were then mapped to the *A. thaliana* genome TAIR10 with Hisat
637   v2.1.0v (Cheng *et al.*, 2017; Kim *et al.*, 2015);. In all samples, well above 85% of the reads
638   mapped to Arabidopsis (**Suppl. Table 2**). Obtained SAM files were sorted and converted to
639   BAM files with the help of samtools v1.6 (Li, 2011; Li *et al.*, 2009). From these files FPKM counts
640   of mapped sequences were derived by StringTie (Pertea *et al.*, 2015).

641   The FPKM-transformed counts were imported in "R" (version 3.4.2, x64) and were $\log_2$
642   transformed by $C_{i,j} = \log_2(FPKM_{i,j} + 1)$, where C is the $\log_2$-transformed FPKM value for
643   gene i (one of 37217 unique transcripts) of sample j (one of three replicates of wild-type mock
644   infected, wild-type infected, *siz1-2* mock infected, or *siz1-2* infected)*.

645   Subsequently, we selected only transcripts that were detected in all 12 samples (C > 0) for
646   further analysis (representing 13114 unique genes). For principal component analysis, we also
647   transformed to data to a $\log_2$-ratio with the mean, by $R_{i,j} = \log_2\left(\frac{FPKM_{i,j}}{\overline{FPKM_i}}\right)$ where R is the $\log_2$-
648   ratio with the mean of transcript i of sample j, and $\overline{FPKM_i}$ is the mean of the FPKM values for
649   gene i.

650   Thereafter, both C and R values were batch-corrected by subtracting the mean
651   difference of the batch from the total mean, as follows

652
$$C_{B,i,j} = C_{i,j} - (\bar{C}_{batch,i} - \bar{C}_{total,i})$$

653
$$R_{B,i,j} = R_{i,j} - (\bar{R}_{batch,i} - \bar{R}_{total,i})$$

654   where C_B and R_B are the batch-corrected values of gene *i* of sample *j* and $\bar{C}_{batch}$ and $\bar{R}_{batch}$
655   are the batch averages, and $\bar{C}_{total}$ and $\bar{R}_{total}$are the averages over the total.

656

657   *Differential expression analysis*

658   To understand the contributing factors underlying variance in the gene expression data, we
659   first used a principal component analysis on R_B to understand the major sources of variance.
660   Thereto we used the *prcomp* function in "R".

661   We then applied a linear model to identify genes contributing to the genotype
662   differences, the differences between mock-infection and infection, and the interaction
663   between both variables, by solving $C_{B,i,j} = G_j + T_j + G_j{\times}T_j + e_j$ where C_B of gene *i* of sample
664   *j* was explained over genotype (G; either wild-type or *siz1-2*) and treatment (T; either mock-

665 infected or infected), the interaction between G and T, and an error-term (*e*). The significances
666 were used to calculate a false discovery rate (FDR) using the *p.adjust* function in "R"
667 (Benjamini & Hochberg, 1995). To make explanatory terms comparable, we applied a single
668 significance threshold of $p < 0.0001$, which corresponded to a FDR of 0.011 for genotype, 0.064
669 for treatment, and 0.131 for the interaction between genotype and treatment.

670   The differentially expressed genes ($p < 0.0001$) were used in an enrichment analysis,
671 as described before (Warmerdam *et al.*, 2019). In short, enrichments were calculated by
672 hypergeometric test, using the TAIR11 databases: Gene ontology, Gene ontology slim, gene
673 classes, and phenotypes (Berardini *et al.*, 2015; Lamesch *et al.*, 2012), and the MapMan gene
674 ontology database, based on TAIR10 (Thimm *et al.*, 2004). We filtered groups were fewer than
675 three genes overlapped, and selected significant enriched groups based on a correction for
676 multiple testing (FDR).

677 *Data availability*

678 The data was submitted to ArrayExpress, under code E-MTAB-8193.

679

680 **Phylogenetic tree**
681 Sequences were aligned in BioEdit v.7.2.6 (Hall, 1999) and a Bayesian tree was created using
682 MrBayes v.3.2.26 (Ronquist *et al.*, 2012). The data set was partitioned according to codon
683 position and the analysis was run for 500,000 generations with a GTR + invariable sites +
684 gamma substitution model using 4 MCMC chains and 4 parallel runs. After checking for
685 conversion with Tracer v.1.7.1 (Rambaut *et al.*, 2018), the burnin was set to 5,000 generations.

686

687 **GpRbp-1 modelling**
688 The model of GpRbp-1 was built by remote homology modelling, using a similar workflow as
689 previously described (Rehman *et al.*, 2009). Briefly, an initial sequence analysis was performed
690 by identifying specific sequence patterns signatures using InterProScan (Jones *et al.*, 2014)
691 and ScanProSite (De Castro *et al.*, 2006). Consensus profiles for structural feature predictions
692 were obtained using various methods, namely Jpred4 (Drozdetskiy *et al.*, 2015), RaptorX-
693 Property (Wang *et al.*, 2016), SCRATCH (Cheng *et al.*, 2005), PsiPred (Buchan & Jones, 2019)
694 and Spider3 (Heffernan *et al.*, 2017) (i.e. secondary structure, intrinsically disorder regions and
695 relative solvent accessibility predictions).

696 The 3D model of GpRbp-1 sequence was built within the interval (aa 61-246) starting from the
697 closest homologues with available crystal structures - namely the IUS-SPRY domain of human
698 RanBP9 (Ran Binding Protein 9, PDB 5JI7) (Hong *et al.*, 2016), mouse RanBP10 (Ran Binding
699 Protein 10, PDB 5JIA) (Hong *et al.*, 2016), and the SPRY domain of human SPRYD3 (SPRY
700 Domain-Containing Protein 3, PDB 2YYO) (Kishishita *et al.*, 2008), sharing 31.5%, 30.9% and
701 20.8% sequence identity respectively with GpRbp-1. The N-terminus region (aa 1 - 60),
702 including the first extended PRY motif was not modeled, as no 3D templates with adequate

703 homology were detected. The model was built using Modeller v9.20 (Webb & Sali, 2014) and
704 further refined by iterative rounds local and global simulated annealing and energy
705 minimization monitored with MolProbity (Williams *et al.*, 2018) until convergence to a
706 Molprobity quality score of 1.11Å from an optimal polypeptide path. The optimized model
707 was further subjected to a 20 ns long molecular dynamics simulation for stability test.
708 Molecular dynamics, simulated annealing and energy minimization stages were performed in
709 explicit solvent in NAMD v2.12 (Phillips *et al.*, 2005) using the CHARMM36M forcefield (Huang
710 *et al.*, 2017), TIP3 water molecules model and a fixed 0.15 M NaCl concentration, with the
711 overall system size summing up to 27050 atoms (from which 2863 atoms correspond to
712 GpRbp-1).

713 MD simulations were performed at 300 K constant temperature, using a 2 fs timestep, Particle
714 Mesh Ewald full-system periodic electrostatics and periodic boundary conditions, Langevin
715 temperature control and Nosé-Hoover Langevin piston for a constant 1 bar pressure control,
716 as implemented in NAMD v2.12 (Phillips *et al.*, 2005). The stability of the model was
717 investigated by analyzing the potential energy, RMSD (root mean square deviations) and RMSF
718 (root mean square fluctuations) along the simulation trajectory. All trajectory analyses and
719 predictive model figures were obtained using VMD (Humphrey *et al.*, 1996) and PyMOL v2.2.3
720 (DeLano, 2002).

721

Acknowledgments
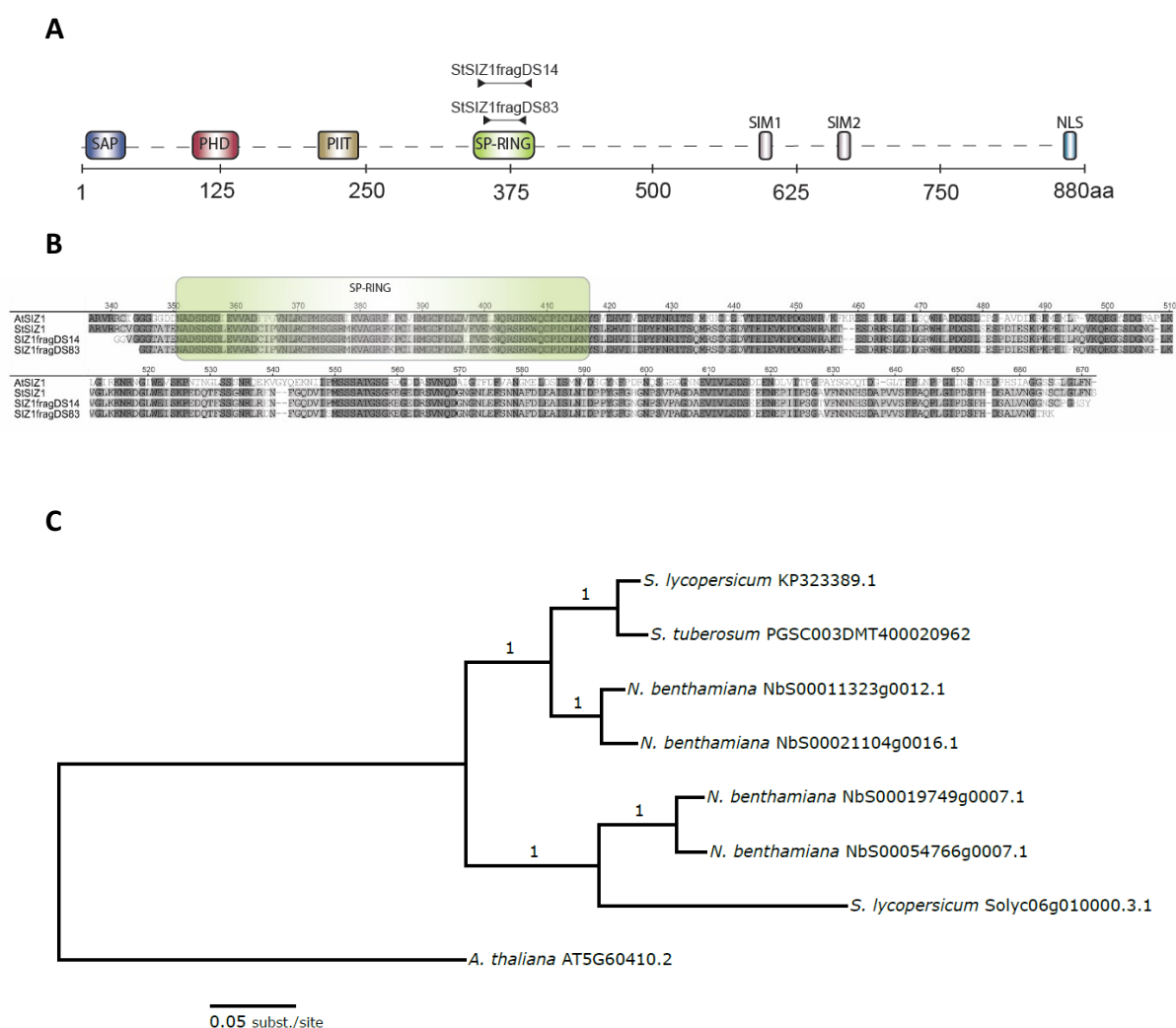731

732 **Figures**

733

734 **Figure 1. GpRbp-1 interacts with fragments encoding the SP-RING domain of StSIZ1. A)** Schematic
735 representation (not to scale) of the domain structure of E3-SUMO ligase SIZ1 from *A. thaliana* (AtSIZ1), indicating
736 the SAP, PHD, PIIT, SP-RING, SIM1 and 2 (SUMO interacting) domains and NLS (Miura *et al.*, 2005; Rytz *et al.*,
737 2018). Arrows indicate the region where the fragments contained in the yeast clones align to AtSIZ1. **B)** Protein
738 alignment of AtSIZ1(TAIR AT5G60410.2), StSIZ1 (XP_006340142.1) and GpRbp-1 interacting fragments
739 (StSIZ1frag14 and StSIZ1frag83). The alignment was generated using a ClustalW algorithm in Geneious (Geneious
740 version 8.1.9) **C)** (Phylogenetic) tree of StSIZ1 (GenBank XM_015314510.1), predicted NbSIZ1 (Solgenomics
741 Niben101Scf05710g03032.1, Niben101Scf05710g03032.1 and Niben101Scf07109g04008.1), SlSIZ1 (GenBank
742 KP323389.1 and Solyc06g010000.3.1) and AtSIZ1 (TAIR AT5G60410.2). The scale indicates substitutions per site.
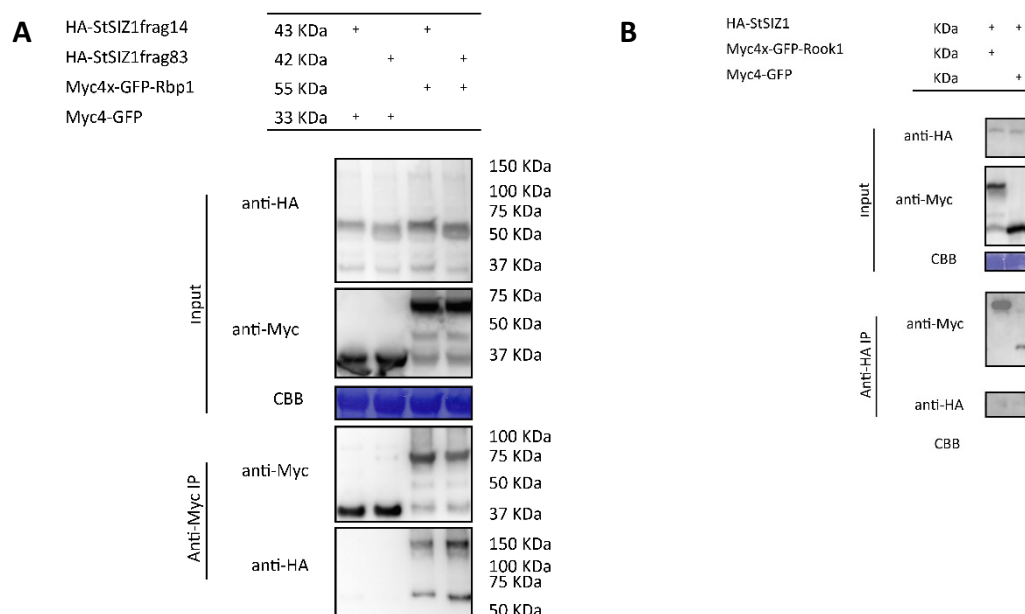
743

744

745
746 **Figure 2. SIZ1 and GpRbp-1 interact *in planta*. A)** Co-immunoprecipitation of epitope tagged StSIZ1 fragments
747 (HA-StSIZ1frag14/83) and GpRbp-1 or (Myc4-GFP-Rbp1) or empty vector control (Myc4-GFP-EV). Pull-down of
748 Myc-GFP-Rbp1 with anti-myc agarose beads results in a specific co-immunoprecipitation of SIZ1 fragments
749 StSIZ1frag14 and StSIZ1frag83. Co-expressing proteins were extracted from *N. benthamiana* leaves 3 days after
750 agroinfiltration. Results are representative of 3 biological repeats and all co-infiltrations contain the silencing
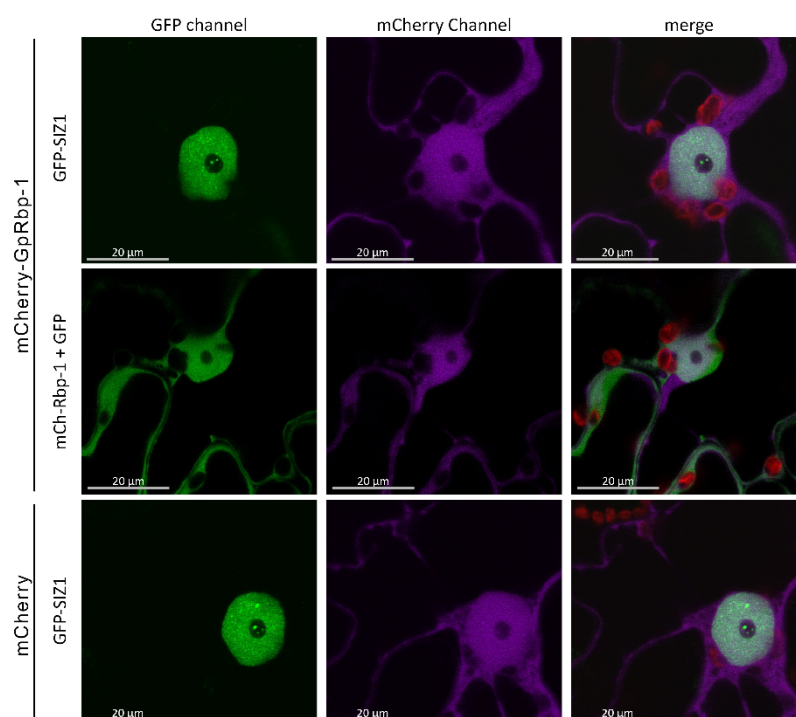751 suppressor p19. **B)** Co-immunoprecipitation of full-length HA-tagged StSIZ (HA-StSIZ1) as in **A).**
752

753
754 **Figure 3. StSIZ1 and GpRpb-1 co-localize to the nucleus of *N. benthamiana* plants.** Live imaging of *N.*
755 *benthamiana* epidermal cells agro-infiltrated with constructs of mCherry tagged GpRbp-1 (mCh-Rbp1) and GFP
756 tagged StSIZ1 (GFP-SIZ1) or GFP and mCh as negative controls. The GFP channel is shown in green and the
757 mCherry in purple. Imaging was performed at 2 dpi, images are representative of 3 biological repeats.
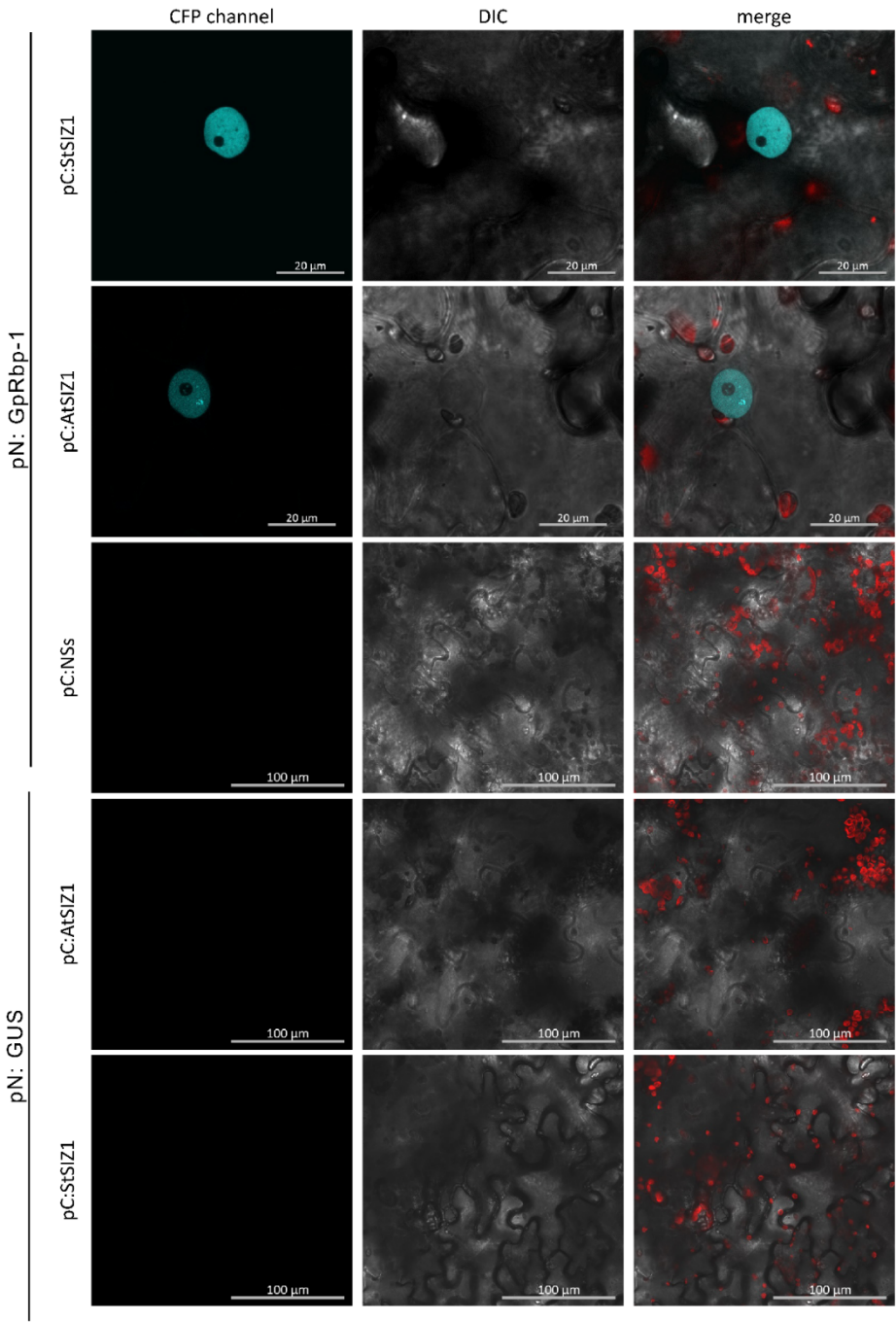
758

759

Figure 4. GpRbp-1 interacts with StSIZ and AtSIZ1 in the nucleus *in planta*. Bimolecular fluorescence complementation of N and C-terminal regions of SCFP3a. SCFP3A amino acids 1-173 were fused to GpRpb-1 (pN:Rbp1) and SCFP3A amino acids 156-239 were fused to StSIZ1(pC:StSIZ1) or AtSIZ1(pC:AtSIZ1) were co-infiltrated to *N. benthamiana* leaves. Co-expression of pN:EV or pC:EV were used as negative controls. The CFP emission channel is shown in blue, light emission in white in the differential interference contrast (DIC) channel and chloroplast auto-fluorescence is shown in red in the merge channel. Results are representative of 2 biological repeats and all co-infiltrations contain the silencing suppressor p19.
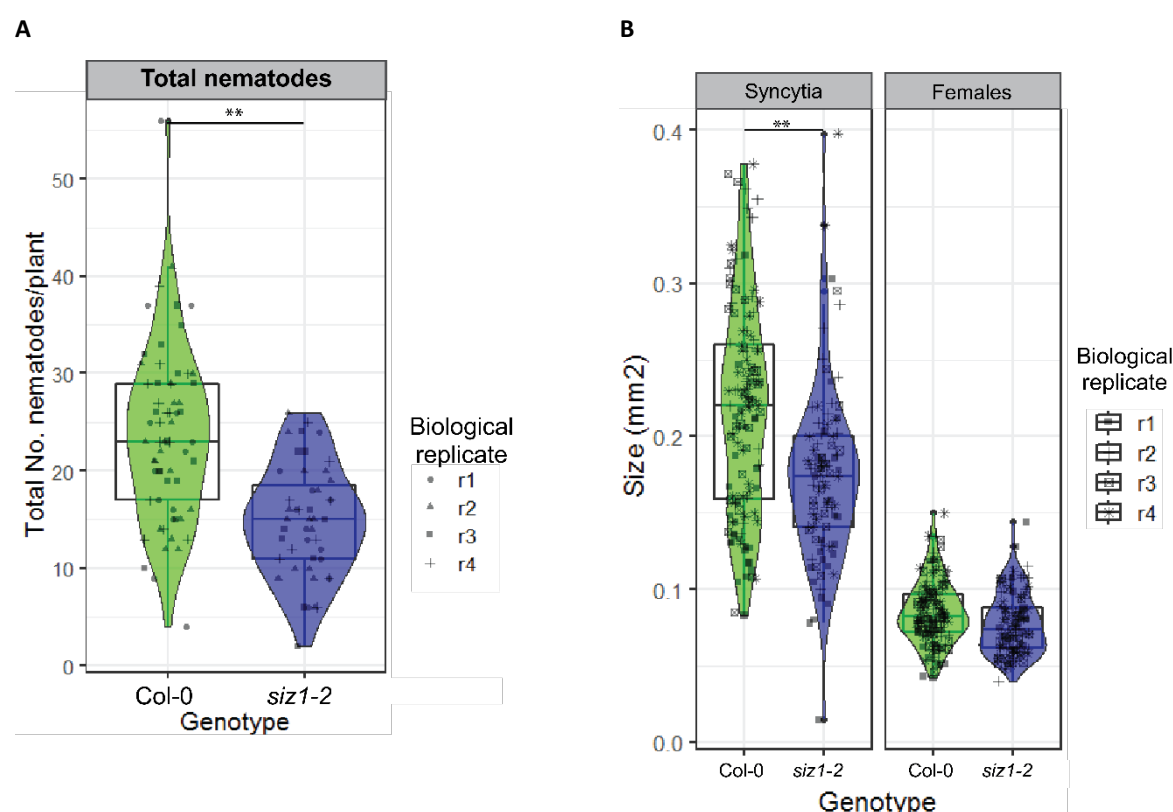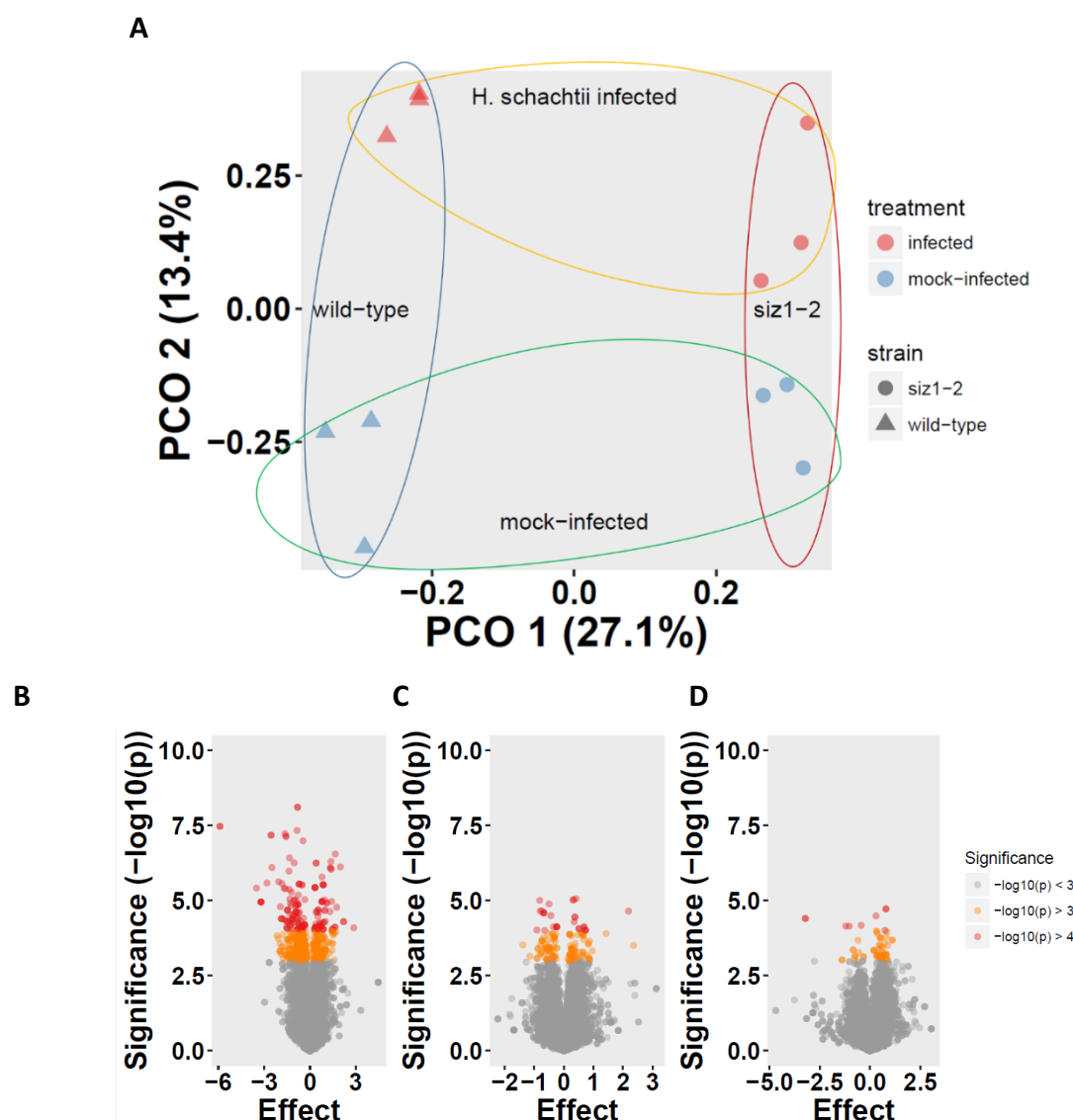
767

Figure 5. **Knock-down of SIZ1 reduces nematode infection in *A. thaliana*. A**) Average number of nematodes per plant in the roots of *Arabidopsis thaliana siz1-2* (n=47) and the background and wild type Columbia 0 (Col-0; n= 65) at 14 dpi. **B**) Average surface area (mm^2) of female nematodes and syncytia present in the roots of *siz1-2* (n=94) and Col-0 (n=128) after 2 weeks of infection. Whiskers indicate the quartile (25 or 75%)+/- 1.5x interquartile range and violin plots describe the distribution of all data points. Stars indicate a significant statistical difference as determined by a one-way ANOVA (**$p < 0.001$). Results are combined measurements from 4 independent biological repeats, using a fixed effects model.
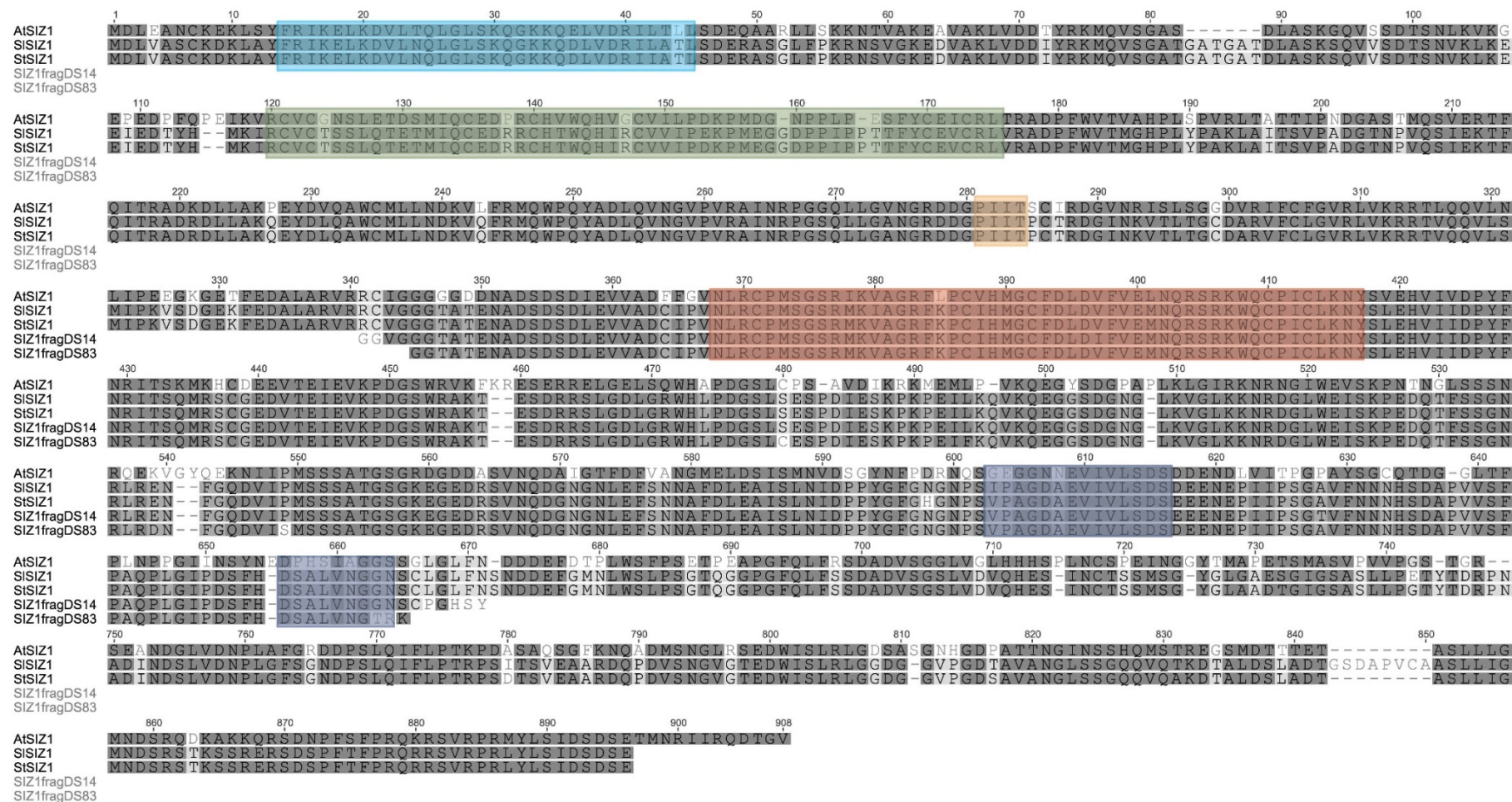
777

Figure 6. The mutation in *siz1-2* plants has a stronger effect in gene expression than nematode infection. A) Principal component analysis of gene expression profiles of *siz1-2* and wild-type Arabidopsis 7 days after (mock) infection with cyst nematodes. The first principal component PCO 1 captures 27.1% of the variation and separates the Arabidopsis seedlings by genotype. The second principal components PCO 2 captures 13% of variation and separates infected from uninfected samples. **B-D)** Volcano plots of differential gene expression as determined by total RNA RNAseq. The x-axis (effect) shows the relative expression of genes. The values on the y-axis reflect the significance of the differences in expression levels. The colours provide a visual aid for the thresholds mentioned in the legend. **B)** Genes differentially regulated in roots of *siz1-2* and wild-type Arabidopsis, irrespective of infection. **C)** Genes differentially regulated by nematode infection, irrespective of genotype. **D)** Genes differentially regulated by infection with *H. schachtii* in roots of *siz1-2* vs wild-type *Arabidopsis* plants, 7 days after inoculation.

Supplementary Figures

Supplemental Table 1. cDNA sequence of StSIZ1 fragments interacting with GpRbp-1 in yeast.

| Prey clone	BLASTX – description	BLASTX - eValue	Sequence
06	E3 SUMO-protein ligase SIZ1, Arabidopsis thaliana	8.936E-95	GGGGGGATGAAAGTTGCTGGAAGATTCAAACCTTGTATACACATGGGCTGCTTTGATCTTGACGTCTTTGTTGAAATGAATCAAAGGTCGAGGAAGTGGCAA TGCCCTATCTGTCTTAAGAACTACTCTTTGGAGCATGTCATCATAGATCCATATTTCAATCGAATTACTTCTCAGATGCGTAGTTGTGGAGAAGATGTCACA GAAATCGAAGTGAAACCTGATGGTTCTTGGCGCGCGAAGACAGAATCTGATCGAAGGAGTCTTGGAGATCTTGGACGTTGGCATTTACCTGATGGGTCTCTG TGTGAATCTCCGGATATAGAGTCGAAGCCTAAGCCTGAAATTTTTAAGCAGGTTAAACAGGAAGGAGGCTCTGATGGAAATGGCCTTAAAGTTGGATTGAAG AAGAACAGAGACGGATTGTGGGAAATCAGCAAACCTGAAGACCAGACATTTTCATCTGGAAATAGATTGAGAGATAATTTTGGTCAGGATGTCATTCCAATG AGCAGCAGTGCCACTGGGAGTGGCAAAGAAGGTGAAGATCGCAGTGTTAATCAGGATGGTAATGGGAACCTTGAATTCTCGAACAATGCATTTGATCTTGAG GCCATCTCTCTTAATATTGACCCACCATATGGTTTTGGCAACGGAAATCCATCGGTACCAGCANGAGATGCTGAAGTTATTGTACTAAGTGATTCTGATGAA
10	E3 SUMO-protein ligase SIZ1, Arabidopsis thaliana	1.057E-107	GGGGGTGTTGGTGGTGGGACAGCCACTGAAAATGCTGATAGCGATAGTGATCTGGAAGTTGTTGCTGATTGTATTCCTGTCAATCTTCGCTGCCCTATGAGT GGTTCAAGGATGAAAGTTGCTGGAAGATTCAAACCTTGTATACACATGGGCTGCTTTGATCTTGACATCTTTGTTGAAATGAATCAAAGGTCGAGGAAGTGG CAATGCCCTATCTGTCTTAAGAACTACTCTTTGGAGCATGTCATCATAGATCCATATTTCAATCGAATTACTTCTCAGATGCGTAGTTGTGGAGAAGATGTC ACAGAAATTGAAGTGAAACCTGATGGTTCTTGGCGCGCGAAGACAGAATCTGATCGAAGGAGTCTTGGAGATCTTGGACGTTGGCATTTACCTGATGGGTCT CTGAGTGAATCTCCAGATATAGAGTCGAAGCCTAAGCCTGAAATTCTTAAGCAGGTTAAACAGGAAGGAGGCTCTGATGGTAATGGCCTTAAAGTTGGATTG AAGAAGAACAGAGACGGATTGTGGGAAATCAGCAAACCTGAAGACCAGACATTTTCATCTGGAAATAGATTGAGAGAAAATTTTGGTCAGGATGTCATTCCA ATGAGCAGCAGTGCCACTGGGAGTGGCAAAGAAGGTGAAGATCGCAGTGTTAATCAGGATGGTAATGGGAACCTTGAATTCTCGAACAATGCATTTGATCTT GAGGCCATCTCTCTTAATATTGACCCACCATATGGTTTTGGCAACGGAAATCCGTCNGTACCAGCAGAGATGCTGAAGTTATTGTACTAAGTGATTCTGAAG AAGANAATGAGCCAATTATCCCATCTGGNACTGTCTTTAATAACANCATAGTGATGCACCTGTAGTTTCNTTTTNCAGCTCAAC
14	E3 SUMO-protein ligase SIZ1, Arabidopsis thaliana	4.2979E-97	GGGGGTGTTGGTGGTGGGACAGCCACTGAAAATGCTGATAGCGATAGTGATCTGGAAGTTGTTGCTGATTGTATTCCTGTCAATCTTCGCTGCCCTATGAGT GGTTCAAGGATGAAAGTTGCTGGAAGATTCAAACCTTGTATACACATGGGCTGCTTTGATCTTGACATCTTTGTTGAAATGAATCAAAGGTCGAGGAAGTGG CAATGCCCTATCTGTCTTAAGAACTACTCTTTGGAGCATGTCATCATAGATCCATATTTCAATCGAATTACTTCTCAGATGCGTAGTTGTGGAGAAGATGTC ACAGAAATTGAAGTGAAACCTGATGGTTCTTGGCGCGCGAAGACAGAATCTGATCGAAGGAGTCTTGGAGATCTTGGACGTTGGCATTTACCTGATGGGTCT CTGAGTGAATCTCCAGATATAGAGTCGAAGCCTAAGCCTGAAATTCTTAAGCAGGTTAAACAGGAAGGAGGCTCTGATGGTAATGGCCTTAAAGTTGGATTG AAGAAGAACAGAGACGGATTGTGGGAAATCAGCAAACCTGAAGACCAGACATTTTCATCTGGAAATAGATTGAGAGAAAATTTTGGTCAGGATGTCATTCCA ATGAGCAGCAGTGCCACTGGGAGTGGCAAAGAANGTGAAGATCGCAGTGTTAATCA
49	E3 SUMO-protein ligase SIZ1, Arabidopsis thaliana	9.617E-116	GGGGGACAGCCACTGAAAATGCTGATAGCGATAGTGATCTGGAAGTTGTTGCTGATTGTATTCCTGTCAATCTTCGCTGCCCTATGAGTGGTTCAAGGATG AAAGTTGCTGGAAGATTCAAACCTTGTATACACATGGGCTGCTTTGATCTTGACGTCTTTGTTGAAATGAATCAAAGGTCGAGGAAGTGGCAATGCCCTATC TGTCTTAAGAACTACTCTTTGGAGCATGTCATCATAGATCCATATTTCAATCGAATTACTTCTCAGATGCGTAGTTGTGGAGAAGATGTCACAGAAATCGAA GTGAAACCTGATGGTTCTTGGCGCGCGAAGACAGAATCTGATCGAAGGAGTCTTGGAGATCTTGGACGTTGGCATTTACCTGATGGGTCTCTGTGTGAATCT CCGGATATAGAGTCGAAGCCTAAGCCTGAAATTTTTAAGCAGGTTAAACAGGAAGGAGGCTCTGATGGAAATGGCCTTAAAGTTGGATTGAAGAAGAACAGA GACGGATTGTGGGAAATCAGCAAACCTGAAGACCAGACATTTTCATCTGGAAATAGATTGAGAGATAATTTTGGTCAGGATGTCATTTCAATGAGCAGCAGT GCCACTGGGAGTGGCAAAGAAGGTGAAGATCGCAGTGTTAATCAGGATGGTAATGGGAACCTTGAATTCTCGAACAATGCATTTGATCTTGAGGCCATCTCT CTTAATATTGACCCACCATATGGTTTTGGCAACGGAAATCCATCGGTACCAGCAGGAGATGCTGAAGTTATTGTACTAAGTGATTCTGATGAAGAGAATGAG CCAATTATCCCATCTGGAGC
83	E3 SUMO-protein ligase SIZ1, Arabidopsis thaliana	3.941E-106	GGGGGACAGCCACTGAAAATGCTGATAGCGATAGTGATCTGGAAGTTGTTGCTGATTGTATTCCTGTCAATCTTCGCTGCCCTATGAGTGGTTCAAGGATG AAAGTTGCTGGAAGATTCAAACCTTGTATACACATGGGCTGCTTTGATCTTGACGTCTTTGTTGAAATGAATCAAAGGTCGAGGAAGTGGCAATGCCCTATC TGTCTTAAGAACTACTCTTTGGAGCATGTCATCATAGATCCATATTTCAATCGAATTACTTCTCAGATGCGTAGTTGTGGAGAAGATGTCACAGAAATCGAA GTGAAACCTGATGGTTCTTGGCGCGCGAAGACAGAATCTGATCGAAGGAGTCTTGGAGATCTTGGACGTTGGCATTTACCTGATGGGTCTCTGTGTGAATCT CCGGATATAGAGTCGAAGCCTAAGCCTGAAATTTTTAAGCAGGTTAAACAGGAAGGAGGCTCTGATGGAAATGGCCTTAAAGTTGGATTGAAGAAGAACAGA GACGGATTGTGGGAAATCAGCAAACCTGAAGACCAGACATTTTCATCTGGAAATAGATTGAGAGATAATTTTGGTCAGGATGTCATTTCAATGAGCAGCAGT GCCACTGGGAGTGGCAAAGAAGGTGAAGATCGCAGTGTTAATCAGGATGGTAATGGGAACCTTGAATTCTCGAACAATGCATTTGATCTTGAGGCCATCTCT CTTAATATTGACCCACCATATGGTTTTGGCAACGGAAATCCATCGGTACCAGCNGNGATGCTGAAGTTATTGTACTAAGTGATTCTGATGAAGAGAATGAGC CAATTATCCCATCTGGAGCTG

793

Supplemental Figure 1. Full-length alignment of StSIZ1, AtSIZ1, SlSIZ1, StSIZ1frag14 and StSIZfrag83. Protein alignment made with the CLUSTALW plugin of Geneious (version 8.1.9) with cost matrix BLOSUM. The characteristic domains of SIZ1 are shown in coloured boxes: the SAP domain in light blue, the PHD domain in green, the PIIT (PINIT) motif in orange, the SP-RING domain in red and the SIMs in dark blue. Full-length proteins were obtained from TAIR, AtSIZ (1009128193) or GenBank StSIZ1 (XP_006340142.1) and SlSIZ1 (KP323389.1). The protein sequences encoded by the yeast-interacting fragments were obtained by automatic translation.

798
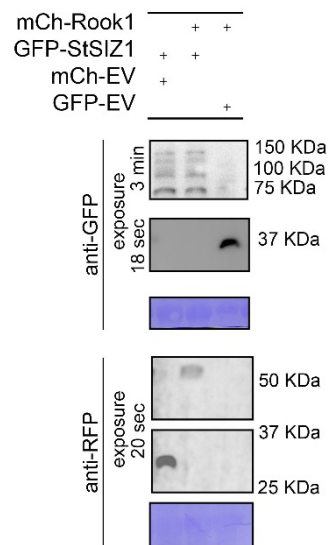
Supplemental Figure 2. Fluorescent fusions of GpRbp-1 and SIZ1 are expressed in leaves of *N. benthamiana*. Western blot detection of fusion of green fluorescent protein with StSIZ1 (GFP-SIZ1), red fluorescent protein mCherry (mCh-GpRbp-1) or GFP and mCh alone. Western blot is performed with anti-GFP and anti-RFP antibodies.
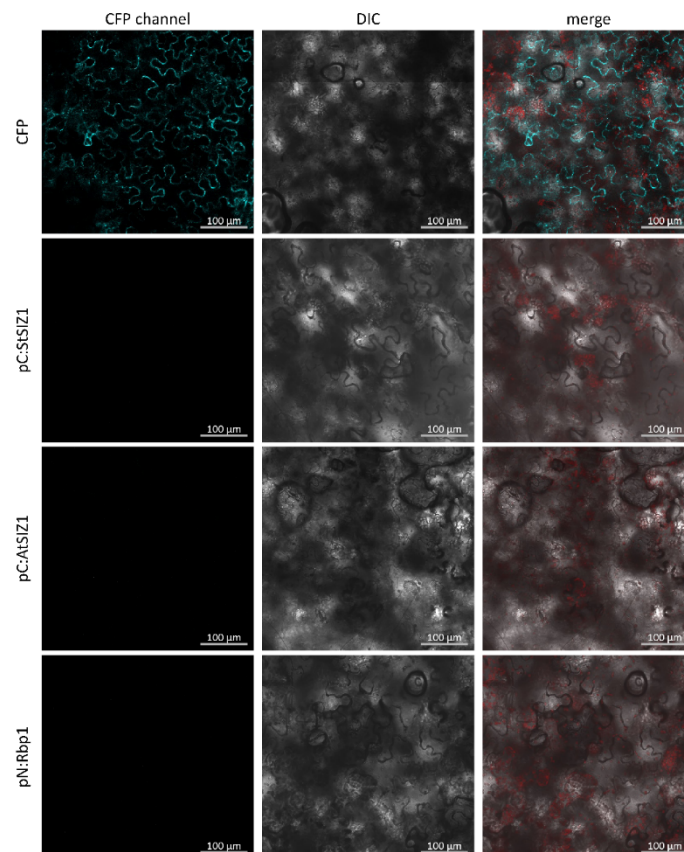
803
Supplemental Figure 3. Individual bimolecular fluorescence complementation constructs do not emit fluorescence when infiltrated individually. Individual N-SCFP3 (pN) or C-SCFP3 (pC) fusions to StSIZ1, GpRbp-1, and. A CFP transformation is shown for comparison of the confocal microscopy settings.
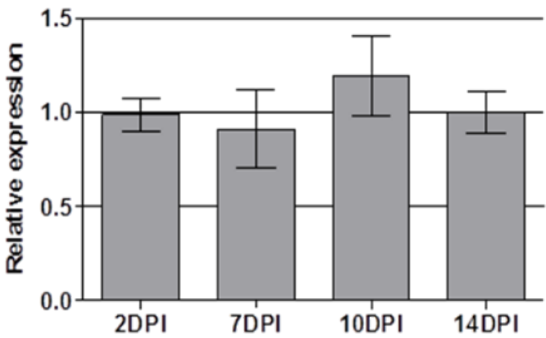
806
807   **Supplemental Figure 4. SIZ1 gene expression during nematode infection of Arabidopsis roots.** AtSIZ1
808   expression as quantified by RT-PCR. Relative expression of AtSIZ1 is calculated relative to the geometric mean of
809   reference genes UBP22 (Hofmann & Grundler, 2007) and UBQ5 (Anwer *et al.*, 2018). Error bars indicate the
810   standard error of 3 independent biological replicates.

811
812
813
814
815
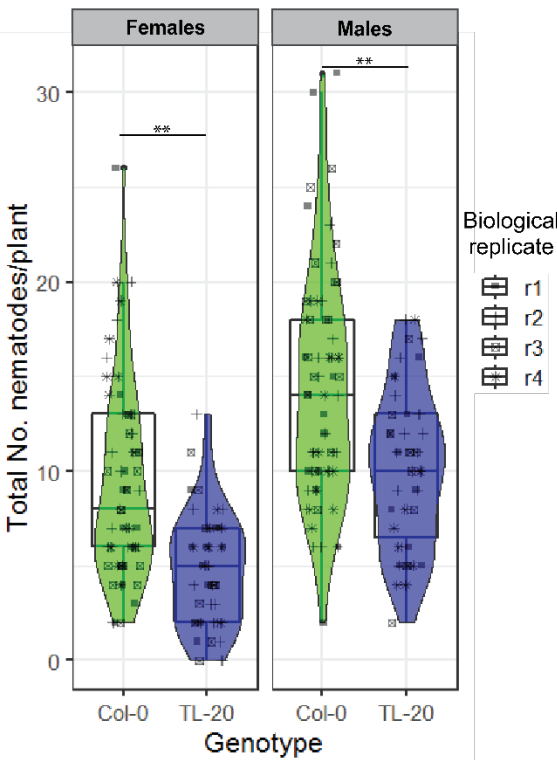
816
817
818   **Supplemental Figure 5. Less *H. schachtii* males and females infect the roots of *siz1-2* Arabidopsis.** Total amount
819   of females and male nematodes present in the roots of *siz1-2* and wild-type (Columbia-0) *Arabidopsis*, after 2
820   weeks of infection. Whiskers indicate the maximum and minimum data points and violin plots describe the
821   distribution of all data points. Results are combined measurements from 4 independent biological repeats. n_{Col-0} = 65 and n_{siz1-2} = 47. Stars indicate statistical significance of the differences in the amount or size of nematodes
822   infecting the roots of *siz1* line and the wild-type control, established by one-way ANOVA, (**p-value<0.001).
824

825 **Supplemental Table 2. HiSat mapping of RNAseq reads to Arabidopsis genome.**

Number	Aligned reads (%)	Multiple aligned reads (%)	Non-aligned reads (%)	Sample name
0	92.76	3.89	3.35	1v2
1	87.83	3.86	8.3	2v2
2	93.33	3.77	2.9	3v2
3	83.68	3.4	12.92	4v2
4	89.92	5.13	4.95	5v2
5	82.08	3.28	14.64	6v2
6	92.32	3.95	3.73	7v2
7	86.23	3.22	10.55	8v2
8	90.44	5.52	4.03	9v2
9	93.66	3.63	2.71	11v2
10	85.71	3.29	11	12v2
11	87.56	4.23	8.21	10v2

826
827
828
829
830
831
832
833
834 **Supplemental Table 3. A list of all the genes significantly regulated in *siz1-2* plants**. geneID indicates the TAIR
835 ID for each entry; the test column indicates which comparison was made; the significance column gives the
836 significance of the difference as determined by the linear model (with FDR correction), the effect column shows
837 the size of the difference in gene expression (log2-units; negative values are lower expressed in col-0, positive
838 values higher expressed in col-0). The significance_FDR column lists the q-values as determined by Benjamini-
839 Hochberg correction. The columns thereafter list properties of the genes.
840
841 Available at; https://drive.google.com/open?id=1YktRjxXNRkLoFI3ZKyjasn UZU-bZ9g28
842
843
844

845 **Supplemental Table 4. Genes significantly regulated by nematode infection and the mutation in *siz1-2* (interaction).** The gene, significance FDR and effect are obtained
846 from Supplemental Table 2. The Gene Symbol, Gene full-name and associated GO annotations were obtained from ThaleMine (Krishnakumar *et al.*, 2014).

Gene ID	Significance FDR	Effect	Gene symbol	Gene full name	Biological process	Molecular function	Cellular compartment
AT3G26550	0.13113341	0.74965		Cysteine/ Histidine-rich C1 domain family protein	no terms	zinc ion binding	nucleus
AT2G45760	0.11601649	-1.03261	BAP2	BON association protein 2	defense response	no terms	membrane
AT3G05936	0.11601649	-1.206		hypothetical protein			
AT4G35620	0.11601649	-0.43799	CYCB2;2	Cyclin B2;2	cell division, regulation of cell cycle, cyclin-dependent protein serine/threonine kinase regulator, ell cycle	protein binding, cyclin-dependent protein serine/threonine kinase regulator activity	nucleus
AT5G40530	0.11601649	-3.21531		S-adenosyl-L-methionine-dependent methyltransferases superfamily protein	rRNA processing, transcription DNA-templated, methylation, covalent chromatin modification, methyltransferase activity	methyltransferase activity	nucleus
AT5G40530	0.11601649	-3.21531		Idem	Idem	Idem	Idem
AT2G17980	0.11601649	0.30137	ATSLY1	Sec1/munc18-like (SM) proteins superfamily	protein secretion, protein transport, vesicle docking suring exocytosis, protein transporter activity	protein transporter	cytosol
AT5G56590	0.11601649	0.79666		O-Glycosyl hydrolases family 17 protein	cell wall organization, defense response	glucan endo-1,3-beta-D-glucosidase activity	anchored component of membrane, plasma membrane, extracellular region
AT5G56590	0.11601649	0.79666		idem	Idem	idem	idem

847

Supplemental Table 5. Gene Ontology categories enriched in genes differentially regulated either by the mutation in *siz1-2 Arabidopsis* or by infection with *H. schachtii*.

Term	Direction	Annotation	Ontology	FDR	Overlap	Overlap expected	Genes in group
Genotype	upregulated in siz1-2	Gene_ontology_slim	cell wall	0.000363	10	0.52545	426
Genotype	upregulated in siz1-2	Gene_ontology_slim	response to abiotic or biotic stimulus	0.000679	21	2.06848	1677
Genotype	upregulated in siz1-2	Gene_ontology_slim	plasma membrane	0.002783	22	2.57543	2088
Genotype	upregulated in siz1-2	Gene_ontology_slim	other binding	0.003769	31	4.30225	3488
Genotype	upregulated in siz1-2	Gene_ontology_slim	response to stress	0.00686	19	2.29544	1861
Genotype	upregulated in siz1-2	Gene_ontology_slim	Transport	0.009484	14	1.55537	1261
Genotype	upregulated in siz1-2	Gene_ontology_slim	transporter activity	0.014674	9	0.88438	717
Genotype	upregulated in siz1-2	Gene_ontology_slim	Extracellular	0.023605	11	1.27291	1032
Genotype	upregulated in siz1-2	Gene_ontology_slim	receptor binding or activity	0.025894	3	0.20105	163
Genotype	upregulated in siz1-2	Gene_ontology	involved in cellular response to ethylene stimulus	8.58E-05	3	0.01974	16
Genotype	upregulated in siz1-2	Gene_ontology	functions in carbohydrate binding	0.000248	4	0.05921	48
Genotype	upregulated in siz1-2	Gene_ontology	involved in defense response to fungus, incompatible interaction	0.000353	3	0.03454	28
Genotype	upregulated in siz1-2	Gene_ontology	located in cell wall	0.000478	8	0.37127	301
Genotype	upregulated in siz1-2	Gene_ontology	involved in response to toxic substance	0.000601	3	0.04810	39
Genotype	upregulated in siz1-2	Gene_ontology	located in plant-type cell wall	0.000601	6	0.22202	180
Genotype	upregulated in siz1-2	Gene_ontology	has carbohydrate binding	0.000639	4	0.09498	77
Genotype	upregulated in siz1-2	Gene_ontology	involved in response to karrikin	0.000767	4	0.10484	85
Genotype	upregulated in siz1-2	Gene_ontology	located in plasma membrane	0.001786	22	2.46688	2000

Genotype	upregulated in siz1-2	Gene_ontology	located in intracellular membrane-bounded organelle	0.004339	3	0.10608	86
Genotype	upregulated in siz1-2	Gene_ontology	located in vacuole	0.004565	7	0.47981	389
Genotype	upregulated in siz1-2	Gene_ontology	involved in ethylene-activated signaling pathway	0.007004	3	0.12581	102
Genotype	upregulated in siz1-2	Gene_ontology	involved in defense response to bacterium	0.007272	4	0.21092	171
Genotype	upregulated in siz1-2	Gene_ontology	involved in defense response	0.013878	5	0.36263	294
Genotype	upregulated in siz1-2	Gene_ontology	has oxidoreductase activity	0.02262	3	0.19118	155
Genotype	upregulated in siz1-2	Gene_ontology	located in cytosol	0.025492	12	1.45053	1176
Genotype	upregulated in siz1-2	Gene_ontology	involved in response to water deprivation	0.028329	3	0.20722	168
Genotype	upregulated in siz1-2	Gene_ontology	has transporter activity	0.028841	3	0.20845	169
Genotype	upregulated in siz1-2	Gene_ontology	located in apoplast	0.030334	4	0.32316	262
Genotype	upregulated in siz1-2	Gene_ontology	involved in signal transduction	0.033703	3	0.21955	178
Genotype	upregulated in siz1-2	Gene_ontology	functions in zinc ion binding	0.038892	4	0.34783	282
Genotype	upregulated in wild-type	Gene_ontology_slim	Extracellular	0.004362	9	0.73792	1032
Genotype	upregulated in wild-type	Gene_ontology_slim	unknown molecular functions	0.024265	13	1.66318	2326
Genotype	upregulated in wild-type	Gene_ontology	functions in sequence-specific DNA binding	0.003638	3	0.09939	139
Genotype	upregulated in wild-type	Gene_ontology	located in extracellular region	0.004785	8	0.61922	866
Genotype	upregulated in wild-type	Gene_ontology	located in membrane	0.007419	8	0.67357	942
Genotype	upregulated in wild-type	Gene_ontology	involved in response to cold	0.010087	3	0.14444	202
Genotype	upregulated in wild-type	Gene_ontology	has molecular_function	0.024225	13	1.66175	2324
Infection	upregulated in infection	Gene_ontology_slim	other binding	0.03602	5	0.56116	3488
Infection	upregulated in infection	Gene_ontology	has protein binding	0.0144	3	0.18325	1139

849
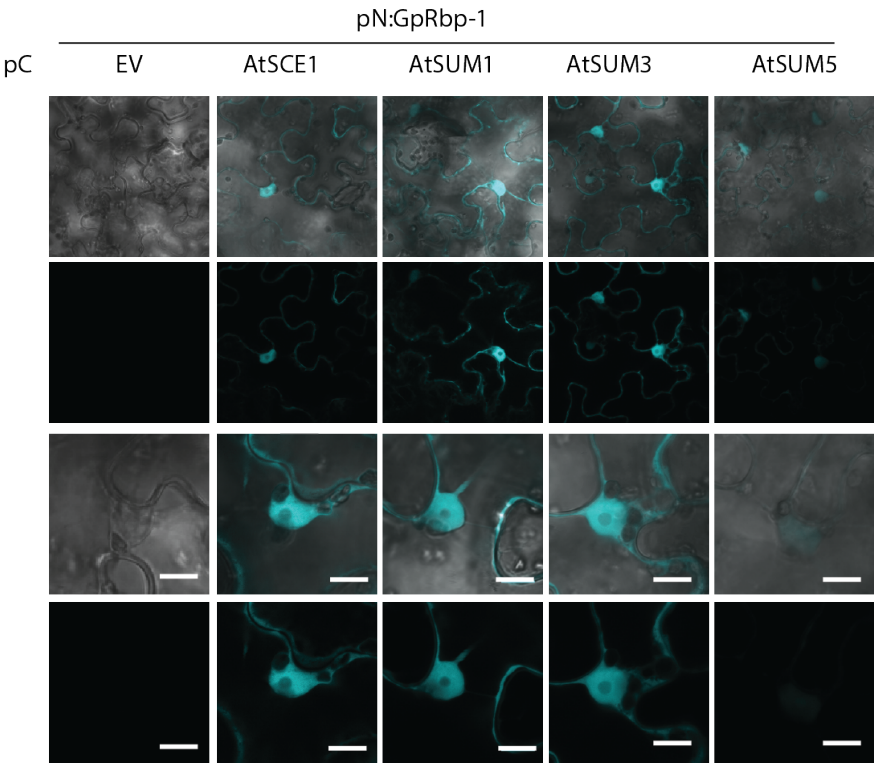
Supplemental Figure 6. Gp-Rbp1 interacts with other members of the SUMO machinery. Bimolecular fluorescence complementation of N and C-terminal regions of SCFP3a. SCFP3A amino acids 1-173 were fused to GbRpb-1 (pN:Gp-Rbp1) and SCFP3A amino acids 156-239 were fused to SUMO1,3,5 or SCE1 (e.g. pC:AtSUM1). The corresponding pN/pC pairs were co-infiltrated to *N. benthamiana* leaves. Co-expression of pN:EV or pC:EV were used as negative controls. The CFP emission channel is shown in blue, light emission in white in the differential interference contrast channel and chloroplast auto-fluorescence is shown in red in the merge channel. Results are representative of 2 biological repeats and all co-infiltrations contain the silencing suppressor p19.

A

Results for putatifs SUMO site [Score: PSmax=18.375 | Cut-off High=12.780 | Cut-off Low=2.460]									
Position K	**Sequence**	**Best PS**	**Consensus direct**			**Consensus Inverted**			
			Type	**PSd**	**DB Hit**	**Type**	**PSi**	**DB Hit**	
K11	MESPKPNKKVKGSSSSGNAEP	0.520	None	0.520		None	0.044	2	
K108	KESGIFYYEVKLSAITASVSI	18.375	None	0.520		Strong consensus inv	18.375		
K123	TASVSIGLATKEMPLDKFVGY	0.069	None	0.015		None	0.069	1	
K164	CSHLNKRPFIKVPKFGEGDVV	1.035	None	1.035	1	None	0.383	1	
K240	PKSADVIEKLKNENLGS----	8.719	Strong Consensus	8.719	2	None	0.057		

Results for putatifs SIM [PSmax=38.183 | Cut-off=0.000]					
Position site	**Sequence**	**Type**	**α/S stretch**	**PS**	**DB Hit**
AA 49-52	TLSETERRLMIVEYTKADWA	SIM Type 2	[Y][SIM][N]	0.000	
AA 74-77	TLSETERRLMIVEYTKADWG	SIM Type 2	[Y][SIM][N]	0.000	

B

ID	Position	Peptide	Score	Cutoff	P-Value	Type
Rook 1	**49 - 53**	**LSETERR LMIVE YTKADWA**	**31.547**	**25.8**	**0.14**	**SUMO Interaction**
Rook 1	56	LMIVEYTKADWACDT	3.144	2.592	0.187	Sumoylation Nonconcensus
Rook 1	**74 - 78**	**LSETERR LMIVE YTKADWG**	**26.714**	**25.8**	**0.171**	**SUMO Interaction**
Rook 1	81	LMIVEYTKADWGCRS	3.348	2.592	0.186	Sumoylation Nonconcensus
Rook 1	219	TVYAPGTKIEANFGP	3.36	2.592	0.109	Sumoylation Nonconcensus
Rook 1	238	KSADVIEKLKNENLG	4.185	2.592	0.044	Sumoylation Nonconcensus
Rook 1	**240**	**ADVIEKLKNENLGS***	**26.804**	**1.534**	**0.001**	**Sumoylation Concensus**

C

861

D

862
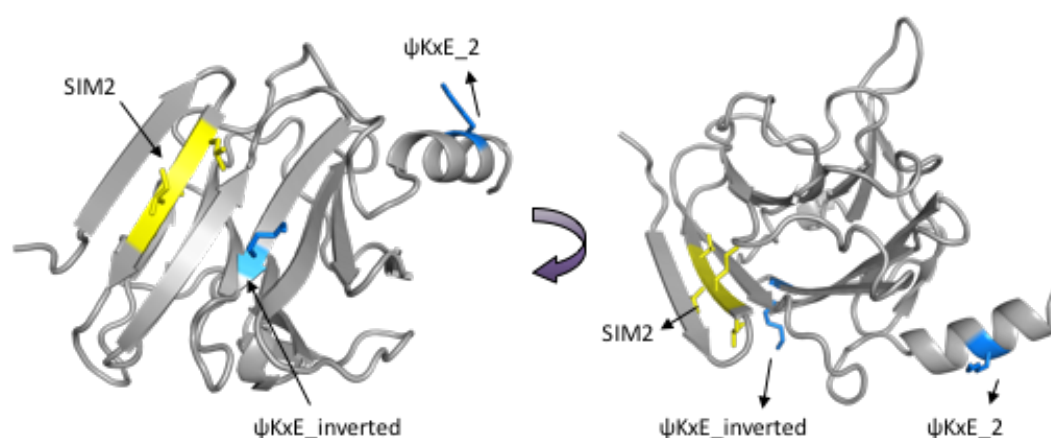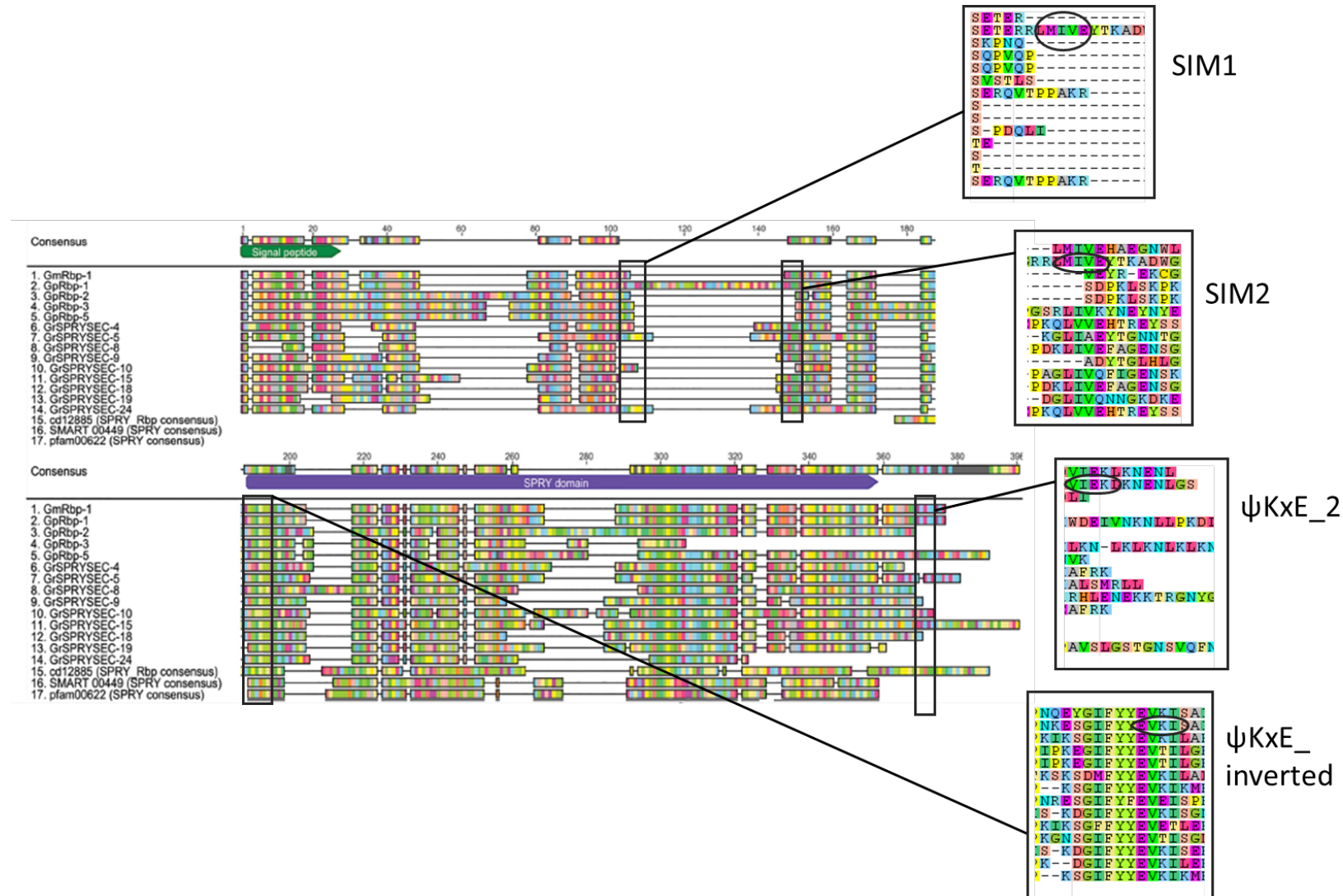
863 **Supplemental Figure 7. SUMOylation and SUMO interacting motifs are predicted in GpRbp-1.** Lysine residues
864 108 and 240 of GpRbp-1 are predicted as SUMOylation sites. The amino acid stretch from position 49 to 53 and
865 from position 74 to 78 of GpRbp-1 are predicted so function as SIMs, using **A)** The Joined Advanced SUMOylation
866 site and SIM Analyser (JASSA) (Beauclair *et al.*, 2015) and **B)** The GPS-SUMO webserver tool (Zhao *et al.*, 2014).
867 **C)** Computational structural model of GpRbp-1 (grey), with SIM2 (yellow), and ψKxE sites indicated (blue).
868 GpRbp-1 was modelled by remote homology modelling from human RBPM10 (PDB: 5JI7) & SPRYD3 (PDB 2YYO)
869 and from mouse RBP9 (PDB: 5J1A). **D.)** Location of SUMO and SIM sites in SPRYSEC alignment (modified from
870 Diaz Granados, *et al*, 2016).

871

872 **Supplemental Table 6. Primers mentioned in the text**

873

Cloning	
Primer name	*Sequence*
GpRbp-1 Forward	5-GGGCCATTACGGCCCAACTCGCTCGCCCAATGGAG-3'
GpRbp -1 Reverse	5-GGGCCGAGGCGGCCCGGCCCATTATAAATTCTCG-3'
iSALK homozygocity *siz1-2* LP	5-GAGCTGAAGCATCTGGTTTTG-3'
iSALK homozygocity *siz1-2* RP	5-CACGACAGATGAAGCATTGTG-3'
F_attB1_AtSCE1	5-GGGGACAAGTTTGTACAAAAAAGCAGGCTCCATGGCTAGTGGAATCGCT-3'
R_attB2_AtSCE1	5-GGGGACCACTTTGTACAAGAAAGCTGGGTATTAGACAAGAGCAGGATACTG-3'
F_attB1_SUM1	5-GGGGACAAGTTTGTACAAAAAAGCAGGCTCAATGTCTGCAAACCAGGAGGAAGACAAG-3'
R_attB2_SUM1GG	5-GGGGACCACTTTGTACAAGAAAGCTGGGTATCAGCCACCAGTCTGATGGAG-3'
F_attB1_SUM3	5-GGGGACAAGTTTGTACAAAAAAGCAGGCTCAATGTCTAACCCTCAAGATGACAAGCCCATC-3'
R_attB2_SUM3GG	5-GGGGACCACTTTGTACAAGAAAGCTGGGTATCAACCACCACTCATCGCCCGGCAC-3'
F_attB1_SUM5	5-GGGGACAAGTTTGTACAAAAAAGCAGGCTCAATGGTGAGTTCCACAGACACAATCTC-3'

R_attB2_SUM5GG	5-GGGGACCACTTTGTACAAGAAAGCTGGGTATCAACCGCCACCAC CAAGTTC-3'
RT-PCR	
Primer name	*Sequence*
At_qPCR_SIZ1_002 F	5-GCTGACGTTTCAGGAGGTTTAGTTG -3'
At_qPCR_SIZ1_001 R	5-GCCTTGTCTTGTCTACTGTCATTCATAC -3'
At_qPCR-UBP22_001_F	5-ACAACATATGACCCGTTTATCGA-3 (Hofmann & Grundler, 2007)
At_qPCR-UBP22_001_R	5-TGTTTAGGCGGAACGGATACT-3
At_qPCR-UBQ5_001_F	5-GTTAAGCTCGCTGTTCTTCAGT-3 (Anwer *et al.*, 2018)
At_qPCR-UBQ5_001_R	5-TCAAGCTTCAACTCCTTCTTTC-3

874

875

876

References

Abad, P., Gouzy, J., Aury, J.-M., Castagnone-Sereno, P., Danchin, E. G. J., Deleury, E.*, et al.* (2008) Genome sequence of the metazoan plant-parasitic nematode Meloidogyne incognita. *Nature Biotechnology,* **26,** 909.

Andrews, S. (2014) FastQC A Quality Control tool for High Throughput Sequence Data.

Anjam, M. S., Shah, S. J., Matera, C., Różańska, E., Sobczak, M., Siddique, S.*, et al.* (2018) Host factors influence the sex of nematodes parasitizing roots of *Arabidopsis thaliana*. *BioRxiv*, 273391.

Anwer, M. A., Anjam, M. S., Shah, S. J., Hasan, M. S., Naz, A. A., Grundler, F. M. W.*, et al.* (2018) Genome-wide association study uncovers a novel QTL allele of AtS40-3 that affects the sex ratio of cyst nematodes in Arabidopsis. *Journal of Experimental Botany,* **69,** 1805-1814.

Augustine, R. C. and Vierstra, R. D. (2018) SUMOylation: re-wiring the plant nucleus during stress and development. *Current opinion in plant biology,* **45,** 143-154.

Beauclair, G., Zamborlini, A., Saïb, A., Bridier-Nahmias, A. and Zagury, J.-F. (2015) JASSA: a comprehensive tool for prediction of SUMOylation sites and SIMs. *Bioinformatics,* **31,** 3483-3491.

Bebber, D. P., Ramotowski, M. A. T. and Gurr, S. J. (2013) Crop pests and pathogens move polewards in a warming world. *Nature Climate Change,* **3,** 985.

Benjamini, Y. and Hochberg, Y. (1995) Controlling the False Discovery Rate: A Practical and Powerful Approach to Multiple Testing. *Journal of the Royal Statistical Society. Series B (Methodological),* **57,** 289-300.

Berardini, T. Z., Reiser, L., Li, D., Mezheritsky, Y., Muller, R., Strait, E.*, et al.* (2015) The arabidopsis information resource: Making and mining the "gold standard" annotated reference plant genome. *Genesis,* **53,** 474-485.

Blanchard, A., Esquibet, M., Fouville, D. and Grenier, E. (2005) Ranbpm homologue genes characterised in the cyst nematodes *Globodera pallida* and *Globodera 'mexicana'*. *Physiological and Molecular Plant Pathology,* **67,** 15-22.

Buchan, D. and Jones, D. T. (2019) The PSIPRED Protein Analysis Workbench: 20 years on. *Nucleic Acids Research*.

Carpentier, J., Esquibet, M., Fouville, D., Manzanares-Dauleux, M. J., Kerlan, M.-C. and Grenier, E. (2012) The evolution of the Gp-Rbp-1 gene in *Globodera pallida* includes multiple selective replacements. *Molecular Plant Pathology,* **13,** 546-555.

Castillo, A. G., Kong, L. J., Hanley-Bowdoin, L. and Bejarano, E. R. (2004) Interaction between a Geminivirus Replication Protein and the Plant Sumoylation System. *Journal of Virology,* **78,** 2758-2769.

Castro, P. H., Verde, N., Lourenco, T., Magalhaes, A. P., Tavares, R. M., Bejarano, E. R.*, et al.* (2015) SIZ1-Dependent Post-Translational Modification by SUMO Modulates Sugar Signaling and Metabolism in Arabidopsis thaliana. *Plant & cell physiology,* **56,** 2297-2311.

Catala, R., Ouyang, J., Abreu, I. A., Hu, Y., Seo, H., Zhang, X.*, et al.* (2007) The Arabidopsis E3 SUMO Ligase SIZ1 Regulates Plant Growth and Drought Responses. *The Plant Cell,* **19,** 2952-2966.

Chen, C. C., Chen, Y. Y., Tang, I. C., Liang, H. M., Lai, C. C., Chiou, J. M.*, et al.* (2011) Arabidopsis SUMO E3 ligase SIZ1 is involved in excess copper tolerance. *Plant Physiology,* **156,** 2225-2234.

Cheng, C. Y., Krishnakumar, V., Chan, A. P., Thibaud-Nissen, F., Schobel, S. and Town, C. D. (2017) Araport11: a complete reannotation of the Arabidopsis thaliana reference genome. *The Plant journal : for cell and molecular biology,* **89,** 789-804.

Cheng, J., Randall, A. Z., Sweredoski, M. J. and Baldi, P. (2005) SCRATCH: a protein structure and structural feature prediction server. *Nucleic acids research,* **33,** W72-W76.

924 **Cheong, M. S., Park, H. C., Hong, M. J., Lee, J., Choi, W., Jin, J. B.*, et al.* (2009) Specific Domain
925   Structures Control Abscisic Acid-, Salicylic Acid-, and Stress-Mediated SIZ1 Phenotypes. *Plant*
926   *Physiology,* **151,** 1930-1942.

927 **Colignon, B., Dieu, M., Demazy, C., Delaive, E., Muhovski, Y., Raes, M.*, et al.* (2017) Proteomic Study
928   of SUMOylation During *Solanum tuberosum-Phytophthora infestans* Interactions. *Molecular*
929   *plant-microbe interactions : MPMI,* **30,** 855-865.

930 **De Castro, E., Sigrist, C. J., Gattiker, A., Bulliard, V., Langendijk-Genevaux, P. S., Gasteiger, E.*, et al.***
931   (2006) ScanProsite: detection of PROSITE signature matches and ProRule-associated functional
932   and structural residues in proteins. *Nucleic acids research,* **34,** W362-W365.

933 **DeLano, W. L.** (2002) Pymol: An open-source molecular graphics tool. *CCP4 Newsletter On Protein*
934   *Crystallography,* **40,** 82-92.

935 **Diaz-Granados, A., Petrescu, A.-J., Goverse, A. and Smant, G.** (2016) SPRYSEC Effectors: A Versatile
936   Protein-Binding Platform to Disrupt Plant Innate Immunity. *Frontiers in Plant Science,* **7**.

937 **Drozdetskiy, A., Cole, C., Procter, J. and Barton, G. J.** (2015) JPred4: a protein secondary structure
938   prediction server. *Nucleic acids research,* **43,** W389-W394.

939 **Elrouby, N., Bonequi, M. V., Porri, A. and Coupland, G.** (2013) Identification of Arabidopsis SUMO-
940   interacting proteins that regulate chromatin activity and developmental transitions. *Proceedings*
941   *of the National Academy of Sciences,* **110,** 19956-19961.

942 **Enders, T. A., Frick, E. M. and Strader, L. C.** (2017) An Arabidopsis kinase cascade influences auxin-
943   responsive cell expansion. *The Plant journal : for cell and molecular biology,* **92,** 68-81.

944 **Fosu-Nyarko, J., Nicol, P., Naz, F., Gill, R. and Jones, M. G. K.** (2016) Analysis of the transcriptome of
945   the Infective stage of the beet cyst nematode, *H. schachtii. PLOS ONE,* **11,** e0147511.

946 **Gheysen, G. and Mitchum, M. G.** (2011) How nematodes manipulate plant development pathways for
947   infection. *Current Opinion in Plant Biology,* **14,** 415-421.

948 **Gheysen, G. and Mitchum, M. G.** (2019) Phytoparasitic nematode control of plant hormone pathways.
949   *Plant physiology,* **179,** 1212-1226.

950 **Gou, M., Huang, Q., Qian, W., Zhang, Z., Jia, Z. and Hua, J.** (2017) Sumoylation E3 Ligase SIZ1
951   modulates plant immunity partly through the immune receptor gene SNC1 in Arabidopsis.
952   *Molecular plant-microbe interactions,* **30,** 334-342.

953 **Guo, R. and Sun, W.** (2017) Sumoylation stabilizes RACK1B and enhance its interaction with RAP2.6 in
954   the abscisic acid response. *Scientific reports,* **7,** 44090-44090.

955 **Hall, T. A.** (1999) BioEdit: a user-friendly biological sequence alignment editor and analysis program
956   for Windows 95/98/NT. In: *Nucleic acids symposium series.* pp. 95-98.

957 **Hammoudi, V., Fokkens, L., Beerens, B., Vlachakis, G., Chatterjee, S., Arroyo-Mateos, M.*, et al.*** (2018)
958   The Arabidopsis SUMO E3 ligase SIZ1 mediates the temperature dependent trade-off between
959   plant immunity and growth. *PLOS Genetics,* **14,** e1007157.

960 **Hansen, L. L., Imrie, L., Le Bihan, T., van den Burg, H. A. and van Ooijen, G.** (2017) Sumoylation of the
961   Plant Clock Transcription Factor CCA1 Suppresses DNA Binding. *Journal of Biological Rhythms,*
962   **32,** 570-582.

963 **Heffernan, R., Yang, Y., Paliwal, K. and Zhou, Y.** (2017) Capturing non-local interactions by long short-
964   term memory bidirectional recurrent neural networks for improving prediction of protein
965   secondary structure, backbone angles, contact numbers and solvent accessibility.
966   *Bioinformatics,* **33,** 2842-2849.

967 **Hirsch, C. D., Hamilton, J. P., Childs, K. L., Cepela, J., Crisovan, E., Vaillancourt, B.*, et al.*** (2014) Spud
968   DB: A resource for mining sequences, genotypes, and phenotypes to accelerate potato Breeding.
969   *The Plant Genome,* **7**.

970   **Hofmann, J. and Grundler, F.** (2007) Identification of reference genes for qRT-PCR studies of gene
971   expression in giant cells and syncytia induced in *Arabidopsis thaliana* by *Meloidogyne incognita*
972   and *Heterodera schachtii*. Nematology, **9.** 317-323

973   **Hong, S. K., Kim, K.-H., Song, E. J. and Kim, E. E.** (2016) Structural basis for the interaction between
974   the IUS-SPRY domain of RanBPM and DDX-4 in germ cell development. *Journal of molecular*
975   *biology,* **428,** 4330-4344.

976   **Huang, J., Rauscher, S., Nawrocki, G., Ran, T., Feig, M., de Groot, B. L.,** *et al.* (2017) CHARMM36: An
977   Improved Force Field for Folded and Intrinsically Disordered Proteins. *Biophysical Journal,* **112,**
978   175a-176a.

979   **Humphrey, W., Dalke, A. and Schulten, K.** (1996) VMD: visual molecular dynamics. *Journal of*
980   *molecular graphics,* **14,** 33-38.

981   **Hussey, R. S.** (1989) Disease-inducing secretions of plant-parasitic nematodes. *Annual review of*
982   *phytopathology,* **27,** 123-141.

983   **Ishida, T., Yoshimura, M., Miura, K. and Sugimoto, K.** (2012) MMS21/HPY2 and SIZ1, two Arabidopsis
984   SUMO E3 ligases, have distinct functions in development. *PloS one,* **7,** e46897-e46897.

985   **Jones, J. T., Kumar, A., Pylypenko, L. A., Thirugnanasambandam, A., Castelli, L., Chapman, S.,** *et al.*
986   **(2009)** Identification and functional characterization of effectors in expressed sequence tags
987   from various life cycle stages of the potato cyst nematode Globodera pallida. *Molecular Plant*
988   *Pathology,* **10,** 815-828.

989   **Jones, P., Binns, D., Chang, H.-Y., Fraser, M., Li, W., McAnulla, C.,** *et al.* (2014) InterProScan 5:
990   genome-scale protein function classification. *Bioinformatics,* **30,** 1236-1240.

991   **Juvale, P. S. and Baum, T. J.** (2018) "Cyst-ained" research into *Heterodera* parasitism. *PLOS Pathogens,*
992   **14,** e1006791.

993   **Kammerhofer, N., Radakovic, Z., Regis, J. M., Dobrev, P., Vankova, R., Grundler, F. M.,** *et al.* (2015)
994   Role of stress-related hormones in plant defence during early infection of the cyst nematode
995   *Heterodera schachtii* in Arabidopsis. *New Phytologist,* **207,** 778-789.

996   **Kim, D., Langmead, B. and Salzberg, S. L.** (2015) HISAT: a fast spliced aligner with low memory
997   requirements. *Nature Methods,* **12,** 357.

998   **Kim, J.-G., Stork, W. and Mudgett, M. B.** (2013) Xanthomonas type III effector XopD desumoylates
999   tomato transcription factor SlERF4 to suppress ethylene responses and promote pathogen
1000   growth. *Cell host & microbe,* **13,** 143-154.

1001   **Kim, J. Y., Jang, I.-C. and Seo, H. S.** (2016) COP1 controls abiotic stress responses by modulating AtSIZ1
1002   function through its E3 Ubiquitin ligase activity. *Frontiers in Plant Science,* **7**.

1003   **Kishishita, S., Uchikubo-Kamo, T., Murayama, K., Terada, T., Chen, L., Fu, Z.Q., Chrzas, J., Shirouzu,**
1004   **M., Wang, B.C., Yokoyama, S**. Crystal sturcture of human SPRY domain. *To be published*.
1005   10.2210/PDB2YYO/PDB

1006   **Krishnakumar, V., Hanlon, M. R., Contrino, S., Ferlanti, E. S., Karamycheva, S., Kim, M.,** *et al.* (2014)
1007   Araport: the Arabidopsis Information Portal. *Nucleic Acids Research,* **43,** D1003-D1009.

1008   **Kurepa, J., Walker, J. M., Smalle, J., Gosink, M. M., Davis, S. J., Durham, T. L.,** *et al.* (2003a) The Small
1009   Ubiquitin-like Modifier (SUMO) protein modification system in Arabidopsis : Accumulation of
1010   SUMO1 and -2 conjugates is increased by stress. *Journal of Biological Chemistry,* **278,** 6862-
1011   6872.

1012   **Kyndt, T., Vieira, P., Gheysen, G. and de Almeida-Engler, J.** (2013) Nematode feeding sites: unique
1013   organs in plant roots. *Planta,* **238,** 807-818.

1014   **Lamesch, P., Berardini, T. Z., Li, D., Swarbreck, D., Wilks, C., Sasidharan, R.,** *et al.* (2012) The
1015   Arabidopsis Information Resource (TAIR): improved gene annotation and new tools. *Nucleic*
1016   *Acids Research,* **40,** D1202-D1210.

Lee, J., Nam, J., Park, H. C., Na, G., Miura, K., Jin, J. B., *et al.* (2006) Salicylic acid-mediated innate immunity in Arabidopsis is regulated by SIZ1 SUMO E3 ligase. *The Plant Journal,* **49,** 79-90.

Li, H. (2011) A statistical framework for SNP calling, mutation discovery, association mapping and population genetical parameter estimation from sequencing data. *Bioinformatics,* **27,** 2987-2993.

Li, H., Handsaker, B., Wysoker, A., Fennell, T., Ruan, J., Homer, N., *et al.* (2009) The Sequence Alignment/Map format and SAMtools. *Bioinformatics,* **25,** 2078-2079.

Lin, J., Mazarei, M., Zhao, N., Zhu, J. J., Zhuang, X., Liu, W., *et al.* (2013) Overexpression of a soybean salicylic acid methyltransferase gene confers resistance to soybean cyst nematode. *Plant biotechnology journal,* **11,** 1135-1145.

Lin, X.-L., Niu, D., Hu, Z.-L., Kim, D. H., Jin, Y. H., Cai, B., *et al.* (2016) An Arabidopsis SUMO E3 Ligase, SIZ1, negatively regulates photomorphogenesis by promoting COP1 activity. *PLOS Genetics,* **12,** e1006016.

Ling, Y., Zhang, C., Chen, T., Hao, H., Liu, P., Bressan, R. A., *et al.* (2012) Mutation in SUMO E3 ligase, SIZ1, disrupts the mature female gametophyte in Arabidopsis. *PLOS ONE,* **7,** e29470.

Martin, M. (2011) Cutadapt removes adapter sequences from high-throuput sequencing reads*, EMBnet.journal,* **17**.

Mascle, X. H., Lussier-Price, M., Cappadocia, L., Estephan, P., Raiola, L., Omichinski, J. G., *et al.* (2013) Identification of a non-covalent ternary complex formed by PIAS1, SUMO1, and UBC9 proteins involved in transcriptional regulation. *The Journal of biological chemistry,* **288,** 36312-36327.

Matunis, M. J., Wu, J. and Blobel, G. (1998) SUMO-1 modification and its role in targeting the Ran GTPase-activating protein, RanGAP1, to the nuclear pore complex. *The Journal of cell biology,* **140,** 499-509.

Mazur, M. J., Kwaaitaal, M., Mateos, M. A., Maio, F., Kini, R. K., Prins, M., *et al.* (2019) The SUMO conjugation complex self-assembles into nuclear bodies independent of SIZ1 and COP1. *Plant Physiology,* **179,** 168-183.

Mei, Y., Thorpe, P., Guzha, A., Haegeman, A., Blok, V. C., MacKenzie, K., *et al.* (2015) Only a small subset of the SPRY domain gene family in is likely to encode effectors, two of which suppress host defences induced by the potato resistance gene. *Nematology,* **17,** 409-424.

Miller, M. J., Scalf, M., Rytz, T. C., Hubler, S. L., Smith, L. M. and Vierstra, R. D. (2013) Quantitative proteomics reveals factors regulating RNA biology as dynamic targets of stress-induced SUMOylation in Arabidopsis. *Molecular & Cellular Proteomics,* **12,** 449-463.

Mitchum, M. G., Hussey, R. S., Baum, T. J., Wang, X., Elling, A. A., Wubben, M., *et al.* (2013) Nematode effector proteins: an emerging paradigm of parasitism. *New Phytologist,* **199,** 879-894.

Miura, K., Lee, J., Gong, Q., Ma, S., Jin, J. B., Yoo, C. Y., *et al.* (2011) *SIZ1* regulation of phosphate starvation-induced root architecture remodeling involves the control of auxin accumulation. *Plant Physiology,* **155,** 1000-1012.

Miura, K., Rus, A., Sharkhuu, A., Yokoi, S., Karthikeyan, A. S., Raghothama, K. G., *et al.* (2005) The Arabidopsis SUMO E3 ligase SIZ1 controls phosphate deficiency responses. *Proceedings of the National Academy of Sciences of the United States of America,* **102,** 7760-7765.

Molendijk, A. J., Ruperti, B., Singh, M. K., Dovzhenko, A., Ditengou, F. A., Milia, M., *et al.* (2008) A cysteine-rich receptor-like kinase NCRK and a pathogen-induced protein kinase RBK1 are Rop GTPase interactors. *The Plant Journal,* **53,** 909-923.

Ng, J. L. P., Perrine-Walker, F., Wasson, A. P. and Mathesius, U. (2015) The control of auxin transport in parasitic and symbiotic root–microbe interactions. *Plants,* **4,** 606-643.

1062 **Nguyen, P. D. T., Pike, S., Wang, J., Nepal Poudel, A., Heinz, R., Schultz, J. C.*, et al.* (2016) The
1063   Arabidopsis immune regulator SRFR1 dampens defences against herbivory by *Spodoptera exigua*
1064   and parasitism by *Heterodera schachtii*. *Molecular plant pathology,* **17,** 588-600.
1065 **Niu, D., Lin, X.-L., Kong, X., Qu, G.-P., Cai, B., Lee, J.*, et al.* (2019) SIZ1-Mediated SUMOylation of TPR1
1066   suppresses plant immunity in Arabidopsis. *Molecular plant,* **12,** 215-228.
1067 **Osterlund, M. T., Hardtke, C. S., Wei, N. and Deng, X. W.** (2000) Targeted destabilization of HY5 during
1068   light-regulated development of Arabidopsis. *Nature,* **405,** 462.
1069 **Pertea, M., Pertea, G. M., Antonescu, C. M., Chang, T.-C., Mendell, J. T. and Salzberg, S. L.** (2015)
1070   StringTie enables improved reconstruction of a transcriptome from RNA-seq reads. *Nature*
1071   *Biotechnology,* **33,** 290.
1072 **Phillips, J. C., Braun, R., Wang, W., Gumbart, J., Tajkhorshid, E., Villa, E.*, et al.* (2005) Scalable
1073   molecular dynamics with NAMD. *Journal of computational chemistry,* **26,** 1781-1802.
1074 **Pieterse, C. M. J., Does, D. V. d., Zamioudis, C., Leon-Reyes, A. and Wees, S. C. M. V.** (2012) Hormonal
1075   Modulation of Plant Immunity. *Annual Review of Cell and Developmental Biology,* **28,** 489-521.
1076 **Piya, S., Binder, B. M. and Hewezi, T.** (2019) Canonical and noncanonical ethylene signaling pathways
1077   that regulate Arabidopsis susceptibility to the cyst nematode *Heterodera schachtii*. *New*
1078   *Phytologist,* **221,** 946-959.
1079 **Quentin, M., Abad, P. and Favery, B.** (2013) Plant parasitic nematode effectors target host defense
1080   and nuclear functions to establish feeding cells. *Frontiers in Plant Science,* **4**.
1081 **Rambaut, A., Drummond, A. J., Xie, D., Baele, G. and Suchard, M. A.** (2018) Posterior summarization
1082   in Bayesian phylogenetics using Tracer 1.7. *Systematic biology,* **67,** 901-904.
1083 **Rehman, S., Postma, W., Tytgat, T., Prins, P., Qin, L., Overmars, H.*, et al.* (2009) A secreted SPRY
1084   domain-containing protein (SPRYSEC) from the plant-parasitic nematode *Globodera*
1085   *rostochiensis* interacts with a CC-NB-LRR protein from a susceptible tomato. *Molecular Plant-*
1086   *Microbe Interactions,* **22,** 330-340.
1087 **Reverter, D. and Lima, C. D.** (2005) Insights into E3 ligase activity revealed by a SUMO–RanGAP1–
1088   Ubc9–Nup358 complex. *Nature,* **435,** 687.
1089 **Rodriguez, M. S., Dargemont, C. and Hay, R. T.** (2001) SUMO-1 Conjugation in vivo requires both a
1090   consensus modification motif and nuclear targeting. *Journal of Biological Chemistry,* **276,** 12654-
1091   12659.
1092 **Ronquist, F., Teslenko, M., Van Der Mark, P., Ayres, D. L., Darling, A., Höhna, S.*, et al.* (2012) MrBayes
1093   3.2: efficient Bayesian phylogenetic inference and model choice across a large model space.
1094   *Systematic biology,* **61,** 539-542.
1095 **Rytz, T. C., Miller, M. J., McLoughlin, F., Augustine, R. C., Marshall, R. S., Juan, Y.-t.*, et al.* (2018)
1096   SUMOylome profiling reveals a diverse array of nuclear targets modified by the SUMO Ligase
1097   SIZ1 during Heat Stress. *The Plant Cell,* **30,** 1077-1099.
1098 **Sacco, M. A., Koropacka, K., Grenier, E., Jaubert, M. J., Blanchard, A., Goverse, A.*, et al.* (2009) The
1099   ncyst nematode SPRYSEC protein RBP-1 elicits Gpa2- and RanGAP2-dependent plant cell death.
1100   *PLOS Pathogens,* **5,** e1000564.
1101 **Sadanandom, A., Bailey, M., Ewan, R., Lee, J. and Nelis, S.** (2012) The ubiquitin–proteasome system:
1102   central modifier of plant signalling. *New Phytologist,* **196,** 13-28.
1103 **Sanchez-Duran, M. A., Dallas, M. B., Ascencio-Ibanez, J. T., Reyes, M. I., Arroyo-Mateos, M., Ruiz-**
1104   **Albert, J.*, et al.* (2011) Interaction between geminivirus replication protein and the SUMO-
1105   conjugating enzyme is required for viral infection. *Journal of Virology,* **85,** 9789-9800.
1106 **Seo, H. S., Yang, J.-Y., Ishikawa, M., Bolle, C., Ballesteros, M. L. and Chua, N.-H.** (2003) LAF1
1107   ubiquitination by COP1 controls photomorphogenesis and is stimulated by SPA1. *Nature,* **423,**
1108   995.

1109 **Seoung Hyun, L., Hyon Jin, P., Choonkyun, J., Hwang Bae, S., Garam, L., Chung Ho, K.*, et al.* (2009)
1110   The Arabidopsis AtLEC gene encoding a lectin-like protein is up-regulated by multiple stimuli
1111   including developmental signal, wounding, jasmonate, ethylene, and chitin elicitor. *Mol. Cells,*
1112   **27,** 75-81.

1113 **Sijmons, P. C., Grundler, F. M. W., Mende, N., Burrows, P. R. and Wyss, U.** (1991) *Arabidopsis thaliana*
1114   as a new model host for plant-parasitic nematodes. *The Plant Journal,* **1,** 245-254.

1115 **Smalle, J. and Vierstra, R. D.** (2004) The ubiquitin 26S proteasome proteolytic pathway. *Annual Review*
1116   *of Plant Biology,* **55,** 555-590.

1117 **Spoel, S. H.** (2018) Orchestrating the proteome with post-translational modifications. *Journal of*
1118   *experimental botany,* **69,** 4499-4503.

1119 **Thimm, O., Bläsing, O., Gibon, Y., Nagel, A., Meyer, S., Krüger, P.*, et al.* (2004) mapman: a user-driven
1120   tool to display genomics data sets onto diagrams of metabolic pathways and other biological
1121   processes. *The Plant Journal,* **37,** 914-939.

1122 **Trudgill, D.** (1967) The effect of environment on sex determination in *Heterodera rostochiensis*.
1123   *Nematologica,* **13,** 263-272.

1124 **van den Burg, H. A., Kini, R. K., Schuurink, R. C. and Takken, F. L. W.** (2010) Arabidopsis Small
1125   Ubiquitin-Like Modifier paralogs have distinct functions in development and defense. *The Plant*
1126   *Cell,* **22,** 1998-2016.

1127 **Verma, V., Croley, F. and Sadanandom, A.** (2018) Fifty shades of SUMO: its role in immunity and at
1128   the fulcrum of the growth–defence balance. *Molecular plant pathology,* **19,** 1537-1544.

1129 **Walsh, C. T., Garneau-Tsodikova, S. and Gatto Jr., G. J.** (2005) Protein posttranslational modifications:
1130   The chemistry of proteome diversifications. *Angewandte Chemie International Edition,* **44,** 7342-
1131   7372.

1132 **Wang, S., Li, W., Liu, S. and Xu, J.** (2016) RaptorX-Property: a web server for protein structure property
1133   prediction. *Nucleic acids research,* **44,** W430-W435.

1134 **Warmerdam, S., Sterken, M. G., Van Schaik, C., Oortwijn, M. E., Lozano-Torres, J. L., Bakker, J.*, et al.*
1135   (2019) Mediator of tolerance to abiotic stress ERF6 regulates susceptibility of Arabidopsis to
1136   *Meloidogyne incognita*. *Molecular plant pathology,* **20,** 137-152.

1137 **Webb, B. and Sali, A.** (2014) Comparative protein structure modeling using MODELLER. *Current*
1138   *protocols in bioinformatics,* **47, 5.6. 1-5.6. 32.**

1139 **Wieczorek, K., Escobar, C. and Fenoll, C.** (2015) Chapter Three - Cell wall alterations in nematode-
1140   infected roots. In: *Advances in Botanical Research.* Academic Press, pp. 61-90.

1141 **Williams, C. J., Headd, J. J., Moriarty, N. W., Prisant, M. G., Videau, L. L., Deis, L. N.*, et al.* (2018)
1142   MolProbity: More and better reference data for improved all-atom structure validation. *Protein*
1143   *Science,* **27,** 293-315.

1144 **Wubben, M. J., Jin, J. and Baum, T. J.** (2008) Cyst nematode parasitism of *Arabidopsis thaliana* is
1145   inhibited by salicylic acid (SA) and elicits uncoupled SA-independent pathogenesis-related gene
1146   expression in roots. *Molecular plant-microbe interactions,* **21,** 424-432.

1147 **Xing, J., Wang, T., Liu, Z., Xu, J., Yao, Y., Hu, Z.*, et al.* (2015) GENERAL CONTROL NONREPRESSED
1148   PROTEIN5-Mediated histone acetylation of FERRIC REDUCTASE DEFECTIVE3 contributes to iron
1149   homeostasis in Arabidopsis. *Plant Physiology,* **168,** 1309-1320.

1150 **Xiong, R. and Wang, A.** (2013) SCE1, the SUMO-conjugating enzyme in plants that interacts with NIb,
1151   the RNA-dependent RNA polymerase of Turnip mosaic virus, is required for viral infection.
1152   *Journal of virology,* **87,** 4704-4715.

1153 **Yang, J., Lin, R., Sullivan, J., Hoecker, U., Liu, B., Xu, L.*, et al.* (2005) Light regulates COP1-mediated
1154   degradation of HFR1, a transcription factor essential for light signaling in Arabidopsis. *The Plant*
1155   *Cell,* **17,** 804-821.

1156 **Yates, G., Srivastava, A. K. and Sadanandom, A.** (2016) SUMO proteases: uncovering the roles of
1157   deSUMOylation in plants. *Journal of Experimental Botany,* **67,** 2541-2548.
1158 **Youssef, R. M., MacDonald, M. H., Brewer, E. P., Bauchan, G. R., Kim, K.-H. and Matthews, B. F.** (2013)
1159   Ectopic expression of AtPAD4 broadens resistance of soybean to soybean cyst and root-knot
1160   nematodes. *BMC plant biology,* **13,** 67.
1161 **Zhang, S., Zhuang, K., Wang, S., Lv, J., Ma, N. n. and Meng, Q.** (2017) A novel tomato SUMO E3 ligase,
1162   SlSIZ1, confers drought tolerance in transgenic tobacco. *Journal of Integrative Plant Biology,* **59,**
1163   102-117.
1164 **Zhao, Q., Jiang, S., Mu, W., Liu, W., Zhao, Y., Xie, Y.*, et al.*** (2014) GPS-SUMO: a tool for the prediction
1165   of sumoylation sites and SUMO-interaction motifs. *Nucleic Acids Research,* **42,** W325-W330.
1166 **Zheng, Y., Chen, Z., Ma, L. and Liao, C.** (2018) The Ubiquitin E3 Ligase RHA2b promotes degradation of
1167   MYB30 in abscisic acid signaling. *Plant Physiol,* **178,** 428-440.